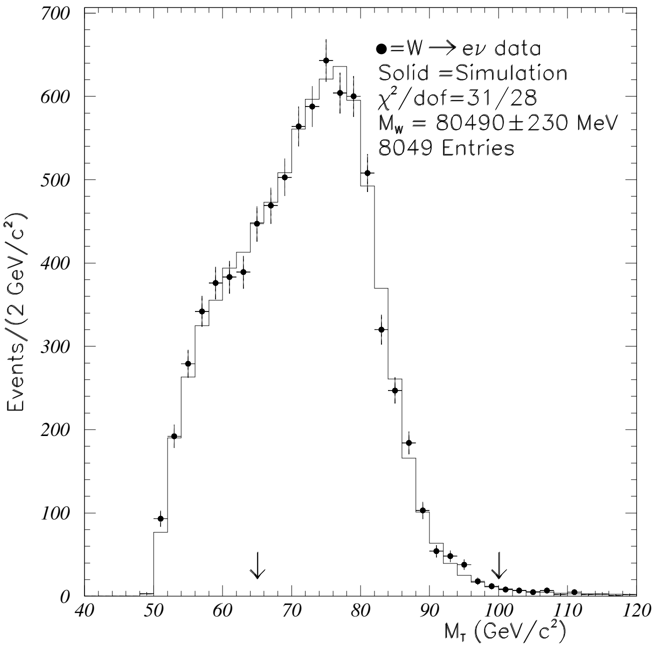

FIG. 43. Transverse mass distribution in $W \to e\nu$ decays. From the CDF collaboration, Frisch, 1995. This distribution is used to measure the W mass by fitting to Monte Carlo expectations; the arrows delimit the range of the fit.

angle between the two transverse momentum vectors, and where we have ignored the mass of the lepton compared to its momentum. Transverse mass distributions, (see Fig. 43), have the following properties : (i) M_T is less than or equal the invariant mass of the lepton-neutrino pair; (ii) M_T distributions are invariant under longitudinal boosts, hence they are independent of the longitudinal momentum of the pair; (iii) they result in Jacobian peaks at the original $l\nu$ invariant mass; (iv) they are fairly insensitive to the total transverse momentum of the pair. (The transverse mass distribution of a pair of invariant mass M and transverse momentum P_T differs from that of a $\mathrm{P}_T = 0$ pair by corrections of order $\approx (\mathrm{P}_T/\mathrm{M})^2$, see for example Barger and Phillips, 1987).

In Fig. 44 we show expected transverse mass distributions for $W+$ jets and $t\bar{t}$, with $\mathrm{M}_{top} = 70$ GeV/c^2. A top signal would result in a significant distortion of the transverse mass spectrum of $W+$ 2 jets events, even after accounting for smearing due to resolution effects (see Section VI). By concentrating on just the shape of the transverse mass distribution, uncertainties due to the theoretical expectation of the $W+$ jets rate do not enter in the analysis. Furthermore, the shape of the transverse mass distribution for the $W+$ jets background is dominated by the kinematics of the $W \to l\nu$ decay, and depends only weakly on the modeling of the W production properties. We note that the transverse mass method can be used to separate a top signal from the $W+$ jets background for both the $t\bar{t}$ and $W \to t\bar{b}$ production mechanisms.

For higher top masses, the $l\nu$ transverse mass distributions in $t\bar{t}$ and $W+$ jets events become indistinguishable, since top quarks will decay into real W bosons. In order to separate signal from background in the lepton + jets mode, one then has to rely on the

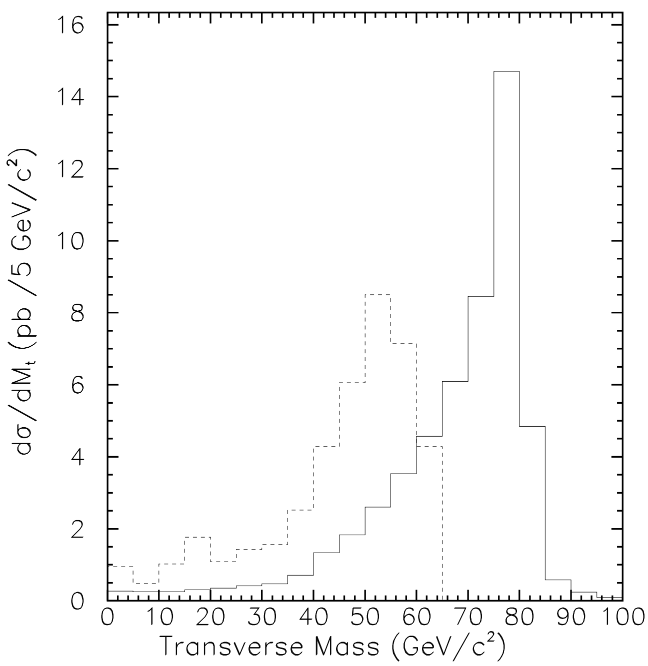

FIG. 44. Expected transverse mass distributions for $W+$ 2 jets (solid) and $p\bar{p} \to t\bar{t} \to$ lepton + 2 jets, for $\mathrm{M}_{top} = 70$ GeV/c^2 (dashed). This is at Tevatron energies (1.8 TeV). The $W+$ 2 jets calculation has been performed with a scale $\mu^2 =< P_T >^2$. Detector and $t\bar{t}$ gluon radiation effects are not included. Relative normalizations are from Monte Carlo. See text for details.

kinematic differences between the two processes, and/or the fact that $t\bar{t}$ events always contain two b-quarks in the final state.

3. Kinematic differences between $t\bar{t}$ and $W+$ jets

Several possible ways of extracting a top signal from the $W+$ jets background using kinematic signatures have been suggested in the literature (Berends *et al.*, 1989; Baer, Barger and Phillips, 1989; Agrawal and Ellis, 1989; Giele and Stirling, 1990; Berends, Tausk, and Giele, 1993; Barger, Ohnemus, and Phillips, 1993; Benlloch, Sumorok, and Giele, 1994; Cobal, Grassmann, and Leone, 1994; Barger *et al.*, 1995). Briefly, the differences between the two processes are the following :

- In $t\bar{t}$ events, the invariant mass of three of the jets should reconstruct to the top mass, and two out of these three jets should have invariant mass equal to the W mass. This is the consequence of the decay chain $t \to Wb$ followed by $W \to q\bar{q}$. Of course no such invariant mass enhancements occurs for the $W+$ jets background.

- Jets in $W+$ jets events tend to have lower transverse momentum than jets in $t\bar{t}$ events. This is due to the fact that jets in W events arise from a brehmstrahlung-like process. For the same reason, these jets also tend to be emitted more in the forward direction than jets from the decay of centrally produced top quarks.

- Top events tend to be more spherical and aplanar than $W+$ jets events. The reason for this is that the QCD $W+$ jets matrix element introduces significant spatial correlations between the jets, e.g. gluon brehmstrahlung ($q \to qg$) and gluon splitting ($g \to q\bar{q}$) favor small opening angles between partons in the final state.

At first glance two-jet and three-jet invariant masses appear to be the most attractive discriminators. Unfortunately, because of the poor jet energy resolution and the number of possible jet combinations that may be present in a given event, this method turns out to be useful only if very large statistics data sets are available. We will not further discuss jet invariant masses in this Section. We will however revisit the issue in Section IX, where the measurements of the top mass will be reviewed.

As an illustration of the kinematic differences between W and top events at the Tevatron, we show the Monte Carlo transverse momentum and pseudorapidity distributions of jets in lepton + 4 jets events for $W+$ 4 jets and $t\bar{t}$ (see Figs. 45, 46, and 47). As anticipated, jets in top events tend to be more central and to have higher transverse momenta. The scalar sum of the transverse momenta of all of the jets in the event is a simple global variable that is expected to provide good discrimination between signal and background, (see Fig. 46).

Note that the choice of scale in the $W+$ jets calculation affects not only the expected rate, but also the shape of kinematic distributions, particularly the jet transverse momentum spectrum. Comparing the distributions for the two equally arbitrary, and a-priori equally reasonable choices, $\mu^2 =< P_T >^2$ and $\mu^2 = \mathrm{M}_W^2$, it is found that the $\mu^2 = \mathrm{M}_W^2$ choice results in a harder jet P_T spectrum, see Figs. 45 and 46. This can simply be understood as follows. The cross-section for a $W+$ N jets event is just given by the convolution of the relevant matrix element with the parton distribution functions. Neglecting the μ^2-dependence of the parton distribution functions, the only scale dependence is due to the factor $\alpha_s^N(\mu^2)$ which appears in the $W+$ N jets matrix element. Because of the running of the strong coupling constant, the choice of an event-by-event scale such as $\mu^2 = < P_T >^2$ results in a higher probability for events with low P_T jets as compared to what one would obtain by choosing a global scale like $\mu^2 = \mathrm{M}_W^2$.

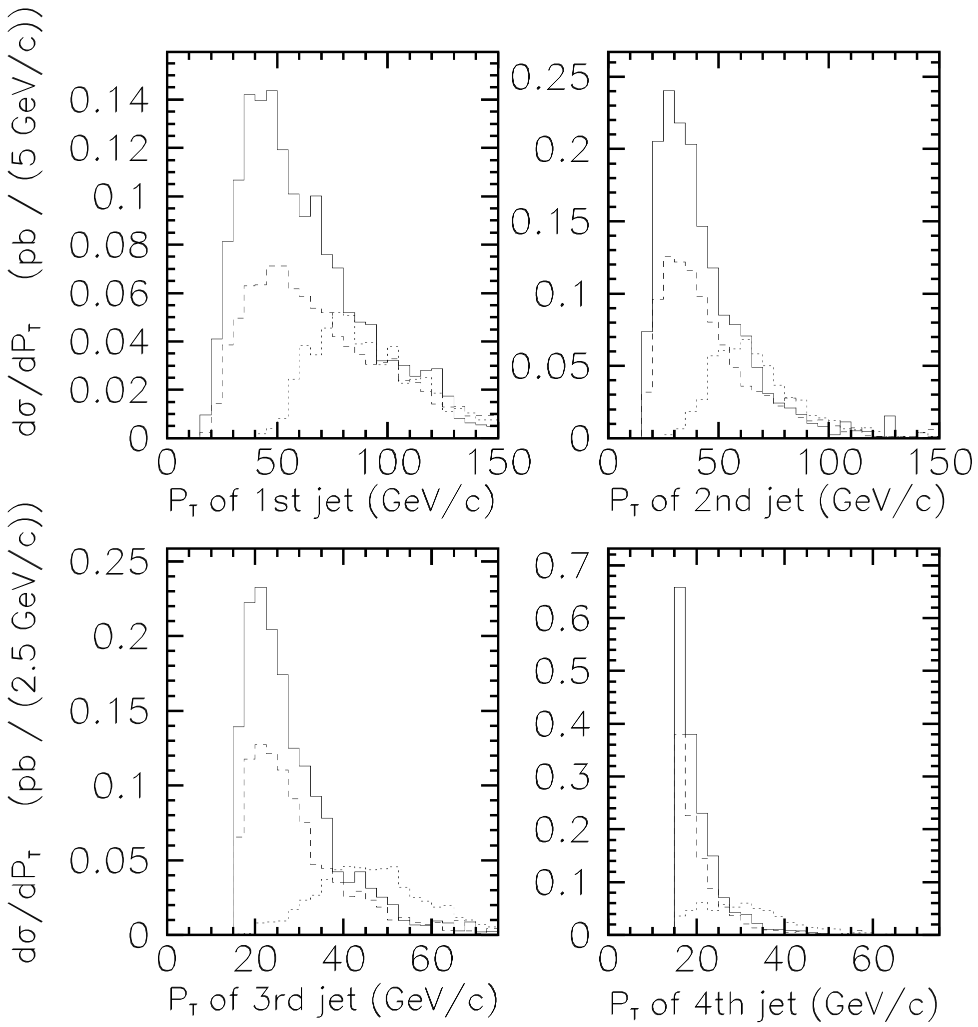

FIG. 45. Expected transverse momentum (P_T) distributions of the first, second, third, and fourth highest P_T jet in $W+$ 4 jets and $t\bar{t}$ events. For $p\bar{p}$ collisions at $\sqrt{s} = 1.8$ TeV. Solid line : $W+$ 4 jets, scale $\mu^2 =< P_T >^2$; dashed line : $W+$ 4 jets, scale $\mu^2 = M_W^2$; dots : $t\bar{t}$, $M_{top} = 170$ GeV/c^2. Note the expanded horizontal scale for the third and fourth jets and that all jets have been required to have $E_T > 15$ GeV. Detector and $t\bar{t}$ gluon radiation effects are not included. See text for details.

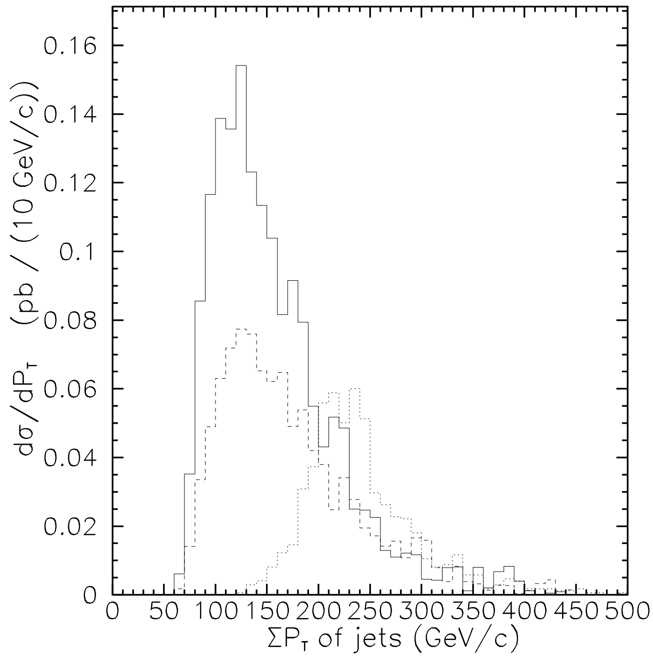

FIG. 46. Expected scalar sum of transverse momenta of 4 jets in $W+$ 4 jets and $t\bar{t}$ events. For $p\bar{p}$ collisions at $\sqrt{s} = 1.8$ TeV. Solid line : $W+$ 4 jets, scale $\mu^2 =< P_T >^2$; dashed line : $W+$ 4 jets, scale $\mu^2 = \mathrm{M}_W^2$; dots : $t\bar{t}$, $\mathrm{M}_{top} = 170$ GeV/c^2. Detector and $t\bar{t}$ gluon radiation effects are not included. See text for details.

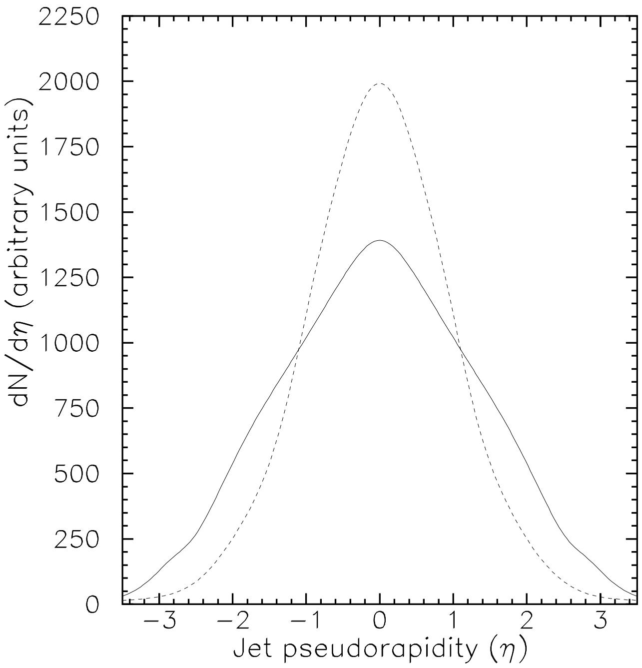

FIG. 47. Pseudorapidity distribution of jets in $W+$ 4 jets and $t\bar{t}$ events. For $p\bar{p}$ collisions at $\sqrt{s} =$ 1.8 TeV. Solid line : $W+$ 4 jets, scale $\mu^2 =< P_T >^2$; dashed line : $t\bar{t}$, $\mathrm{M}_{top} = 170$ GeV/c^2.

Another discriminant that can be employed is *aplanarity*. Aplanarity is defined as $\mathcal{A} \equiv 3/2\lambda_1$, where λ_1 is the smallest eigenvalue of the matrix $M_{ab} = \sum P_a P_b / \sum P^2$, where P_i are the cartesian components of momentum of the parton, P is the magnitude of the three-momentum, and the sum is over all final state objects: jets, electrons, muons, and neutrinos. Zero aplanarity corresponds to planar events. $W+$ jets events are expected to be more planar than $t\bar{t}$ events, (see Fig. 48).

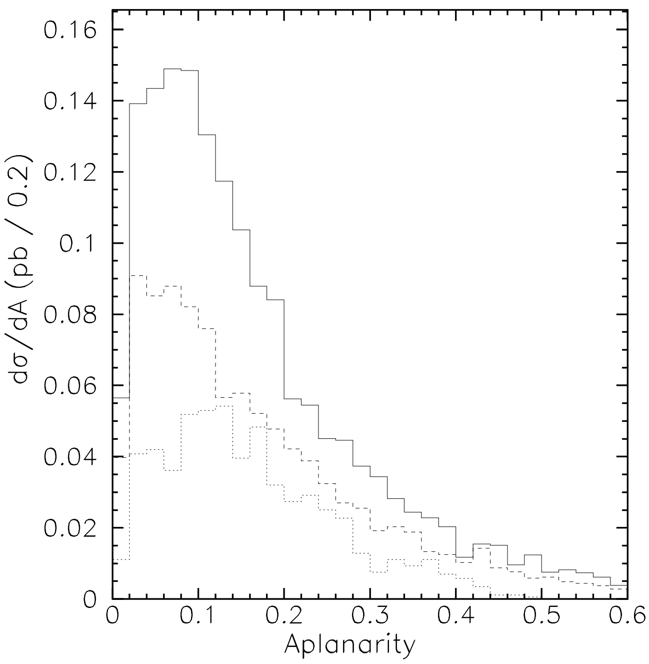

FIG. 48. Expected aplanarity for $W+$ 4 jets and $t\bar{t}$ events. For $p\bar{p}$ collisions at $\sqrt{s}$ = 1.8 TeV. Solid line : $W+$ 4 jets, scale $\mu^2 = < P_T >^2$; dashed line : $W+$ 4 jets, scale $\mu^2 = \mathrm{M}_W^2$; dots : $t\bar{t}$, M_{top} = 170 GeV/c^2. Aplanarity here is calculated in the laboratory frame from the four jets, the lepton, and the neutrino. Detector and $t\bar{t}$ gluon radiation effects are not included. See text for details.

It is clear from this discussion that in order to extract a top signal from kinematic distributions, special attention must be payed to the systematic uncertainties associated with the theoretical modeling of the $W+$ jets backgrounds. The theoretical uncertainties can be bounded by comparing the data with theoretical predictions in kinematic regions where the top signal is small, e.g. in samples of events with low jet multiplicity and/or low transverse momentum jets. Deviations from the $W+$ jets expectations in kinematic regions where the top quark is expected to contribute would then signal the presence of $t\bar{t}$ events in the sample (or possibly of some other source of $W+$ jets events beyond standard QCD production).

Samples of $Z+$ jets events in principle provide the ideal testing ground for the $W+$ jets calculation. Unfortunately, at $\sqrt{s}$ = 1.8 TeV the cross-section for $p\bar{p} \to Z$ is a factor of 3.3 smaller than that for $p\bar{p} \to W$. Furthermore, the leptonic branching ratio of the Z is also a factor of three smaller than that of the W. As a result, the number of reconstructed Z events is approximately one order of magnitude smaller than that of W events. Because of the limited statistics, Z events, although useful as a first order check, do not provide stringent bounds on the modeling of vector boson + $\geq$ 3 jets production. We will discuss these issues in more detail in Section VIII, where the experimental results will be reviewed.

4. b-quark tagging

An alternative method that can be employed to separate the $t\bar{t}$ signal from the $W+$ jets background is to *tag* the b-quarks in top events. Each $t\bar{t}$ event contains one b- and one $\bar{b}$-quark from the decays $t \to Wb$ and $\bar{t} \to W\bar{b}$, whereas the jets in W events arise mostly from the fragmentation of gluons and light quarks.

There are two ways to detect the presence of b-quarks. The first method is based on the detection of additional leptons from the semileptonic decays $b \to cl\nu$ or $b \to c \to sl\nu$. The semileptonic branching ratios of bottom and charm quarks are approximately 10% per lepton species (Montanet *et al.*, 1994). There is on average about one lepton (electron + muon) from b or c decay in each top event, where we have also included the contributions from c-quarks from $W \to c\bar{s}$, which occurs in one half of all hadronic W decays. From an experimental point of view, detection of these leptons is more difficult than detection of leptons from W decays, because these leptons tend to have a much lower transverse momentum (compare Figs. 49 and 29). Furthermore, these leptons are not isolated but are accompanied by nearby hadrons from the b-quark fragmentation and the b-hadron decay. This makes efficient detection of electrons particularly challenging.

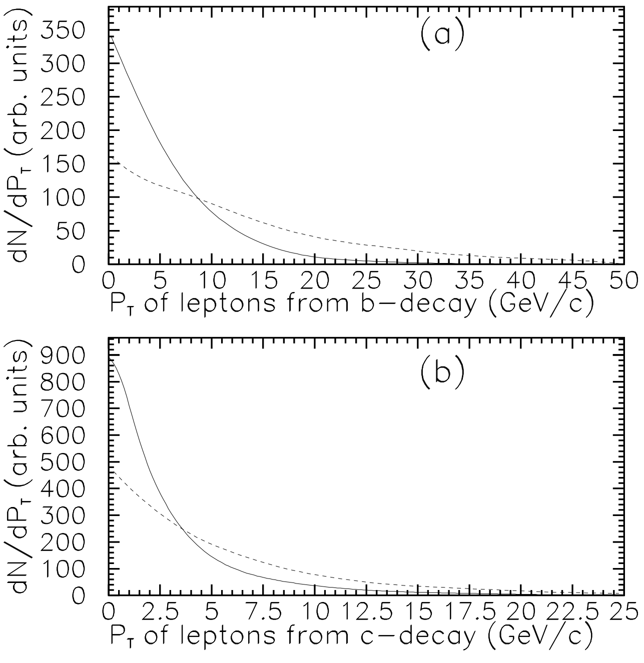

FIG. 49. (a) Expected transverse momentum of leptons from $t \to b \to cl\nu$ Solid line : M_{top} = 110 GeV/c^2; dashed line : M_{top} = 170 GeV/c^2. (b) Same as (a), but for $t \to b \to c \to sl\nu$. For $p\bar{p} \to t\bar{t}$ at $\sqrt{s}$ = 1.8 TeV, from the ISAJET Monte Carlo generator. Note the different horizontal scales in (a) and (b).

Bottom and charm quarks can also be tagged by exploiting the long lifetime of b- and c-hadrons. The recent compilation from the Particle Data Group (Montanet *et al.*) reports a lifetime of 1.537 $\pm$ 0.021 ps for b-hadrons, and 0.415 $\pm$ 0.004 ps and 1.057 $\pm$ 0.015 ps for neutral and charged D mesons respectively. As a consequence of the long lifetime, b-hadrons in a top event are expected to travel several mm before decaying, (see Fig. 50). With the advent of silicon microstrip-vertex detectors, the position of decay vertices can be measured with resolutions of order 100-150 μm. It then becomes possible to separate with good efficiency the secondary vertex where the b-decay occurs from the primary $p\bar{p}$ interaction point.

There are two main sources of background to the lepton- or vertex-tagged $t\bar{t}$ signal. The first one is instrumental. Hadrons originating from the fragmentation of gluons and light quarks in $W+$ jets events can be misidentified as muons or electrons. This happens for example when hadronic showers in the calorimeter fluctuate to mimic the electron signature, or when kaons and pions decay to muons. Also, track mismeasurements or decays of other long-lived particles such as Λ and K_s can result in the reconstruction of spurious detached vertices. Needless to say, these effects have to be considered very carefully. As we will discuss in Section VIII, sufficiently good instrumental background rejection has been achieved, and methods to precisely estimate the remaining background have been developed.

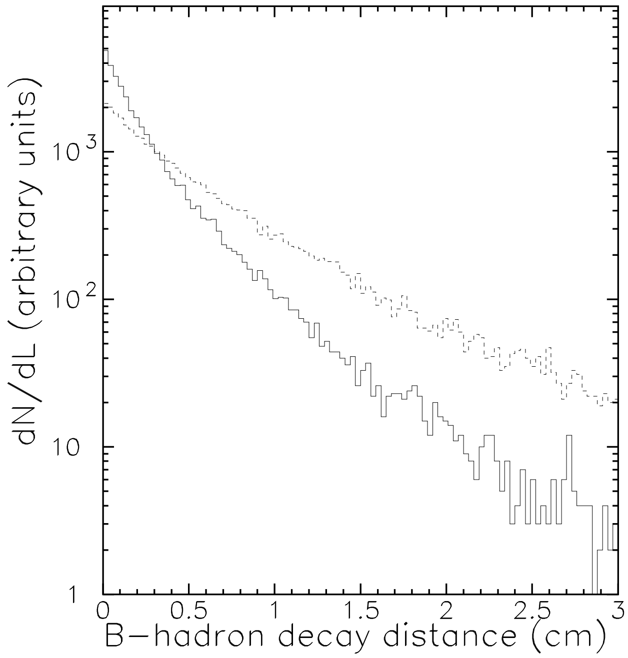

FIG. 50. Distance travelled by b-hadrons in top events before decaying. Solid line : M_{top} = 110 GeV/c^2; dashed line : M_{top} = 170 GeV/c^2. This distance is calculated by convoluting the momentum spectrum of b-hadrons from the ISAJET $p\bar{p} \to t\bar{t}$ ($\sqrt{s}$ = 1.8 TeV) Monte Carlo with their lifetime.

The second background source stems from the fact that a small fraction of jets in $W+$ jets events will contain heavy-quarks (b or c). In the absence of additional kinematic information, these events constitute an irreducible physical background to the lepton + jets + b-tag

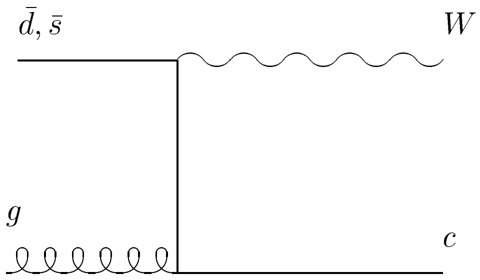

FIG. 51. Lowest order Feynman diagram for production of $W+$ charm in $p\bar{p}$ collisions. At higher order, $gg \to Wc\bar{s}$ diagrams also contribute.

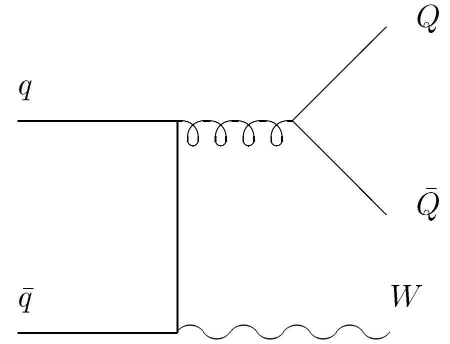

FIG. 52. Lowest order Feynman diagram for production of $WQ\bar{Q}$ in $p\bar{p}$ collisions. $Q = c$ or b.

$t\bar{t}$ signature which needs to be carefully evaluated. A comprehensive discussion of these backgrounds, in the context of the CDF experiment, is given by F. Abe *et al.*, 1994a, and will be summarized below. The discussion here applies equally well to lepton or vertex b-tagging methods.

Heavy-quarks in $W+$ jets event can be produced singly, in the process $\bar{s}g \to Wc$ or $\bar{d}g \to Wc$, (see Fig. 51), or in pairs, when a gluon in a $W+$ jets event *splits* into a $c\bar{c}$ or $b\bar{b}$ pair, (see Fig. 52). The gluon splitting probability, $g \to Q\bar{Q}$, $Q = c$ or b, is estimated to be of order a few percent, with significant theoretical uncertainties (Mangano and Nason, 1992; Müller and Nason, 1985 and 1986). Experimental extractions of the $g \to c\bar{c}$ probability in both $p\bar{p}$ (Ikeda, 1990, F. Abe *et al.*, 1990d) and e^+e^- collisions (Akers, 1995) are found to be in agreement with the results of the theoretical calculations, within the large experimental and theoretical uncertainties. In what follows we will refer to these two processes as Wc and $WQ\bar{Q}$ respectively.

The Wc background estimation begins by computing the fraction of $W+$ jets events that contain a single c-quark, from diagrams like the one shown in Fig. 51, using the VECBOS and HERWIG event generators. This fraction is found to be of order 8%, with small variations depending on the jet multiplicity and the choice of the input parton distribution function for strange quarks in the proton. To obtain an absolute background prediction, this fraction is then multiplied by the number of observed $W+$ jets event and the tagging efficiency for c-quarks. The tagging efficiency for these events clearly depends on the details of the tagging algorithm. However, it is in general much smaller (typically by a factor of order 5) than the tagging efficiency for $t\bar{t}$ since (i) the tagging efficiency for c-quarks is lower than that of b-quarks because e.g. there are fewer tracks in a c decay than in a b decay, and (ii) there are multiple b- and c-quarks in a top event that can potentially be tagged. Therefore, as a result

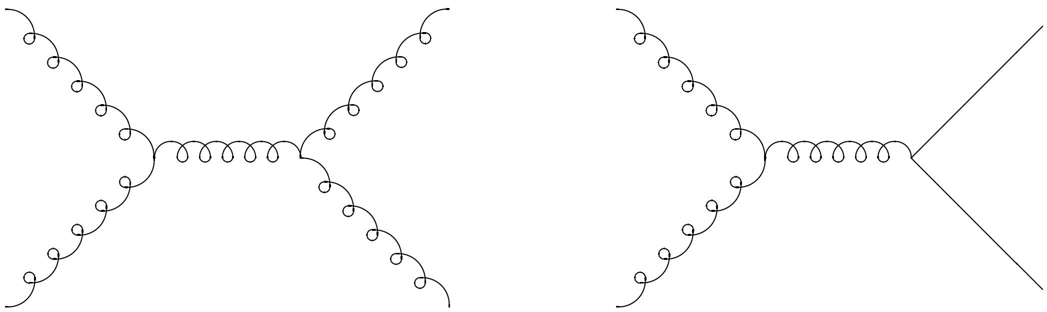

FIG. 53. Two of the possible LO Feynman diagrams for jet production in $p\bar{p}$ collisions: $gg \to gg$ and $gg \to q\bar{q}$.

of the small probability for a Wc event and its small tagging efficiency, the Wc background is much smaller than the expected tagged $t\bar{t}$ rate. The highly uncertain overall normalization of the $W+$ jets theoretical calculation does not enter in the background estimate, since only the **fraction** of Wc events is taken from theory.

The $WQ\bar{Q}$ background is more important because the tagging efficiency for $Wb\bar{b}$ is comparable to that of $t\bar{t}$. This background can be estimated in two ways. The first method (*Method I*) requires a minimum of theoretical input, and is expected to yield an overestimate of the $WQ\bar{Q}$ background. The alternative method, (*Method II*), is based on the state-of-the-art theoretical understanding of heavy quark production,

At the heart of the Method I background calculation is the assumption that the heavy flavor content (b or c) of jets in $p\bar{p} \to$ jets (*generic-jets*, see Fig. 53) is the same or larger than the heavy flavor content of jets in $W+$ jets events. Accepting this assumption for now, we proceed to describe the Method I background calculation.

The generic-jet sample includes gluon and light-quark jets, as well as a small fraction of heavy-quark jets. A generic-jet can be tagged due to instrumental effects resulting in a false tag of a light-quark or gluon jet, or due to the b- or c-quark contribution. Operationally, a *tag-rate* is measured for generic-jets as the probability of tagging a generic-jet as a function of several relevant variables (e.g. jet P_T, track multiplicity). The generic-jet tag-rate is then applied to the sample of jets in $W+$ jets events, to predict an upper limit for the sum of the instrumental and $WQ\bar{Q}$ backgrounds to the $t\bar{t} \to W+$ jets $+$ b-tag signature. From an experimental point of view this has the advantage that both the instrumental and $WQ\bar{Q}$ backgrounds are estimated simultaneously directly from the data. No a-priori knowledge of the tagging efficiency, or the $WQ\bar{Q}$ content of the sample, is needed.

We now turn to a discussion of the theoretical assumption on which the Method I $WQ\bar{Q}$ background calculation is based. At Tevatron energies, generic-jets in the relevant P_T range (20-150 GeV/c) consist predominantly of gluon-jets. There will also of course be a contribution from light-quark jets as well as $p\bar{p} \to Q\bar{Q}$. The lowest order Feynman diagrams for direct production of $b\bar{b}$ and $c\bar{c}$ pairs in $p\bar{p}$ collisions are identical to the ones for $t\bar{t}$ production shown in Fig. 16. For the b- and c-quarks however, it is found that higher order diagrams such as the ones displayed in Fig. 54 contribute a very significant amount to the $p\bar{p} \to Q\bar{Q} + X$ cross-section. For instance, the gluon splitting diagram is believed to account

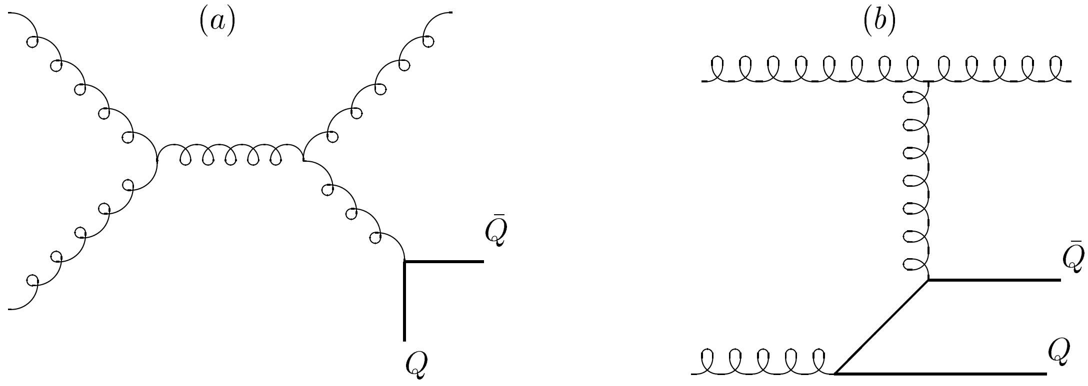

FIG. 54. Higher order Feynman diagrams for $Q\bar{Q}$ production in $p\bar{p}$ collisions: (a) gluon splitting; (b) flavor excitation.

for of order 70% of the $b\bar{b}$ and $c\bar{c}$ production rate (Mangano, Nason, and Ridolfi, 1992).

The heavy-flavor content of generic-jets is expected to be higher than that of jets in $W+$ jets events for two reasons : (i) in $W+$ jets events there are no contributions from lowest order, direct, $Q\bar{Q}$ production (Fig. 16) and next-to-leading order flavor excitation (Fig. 54b), and (ii) generic-jets consist mostly of gluon jets which can result in $Q\bar{Q}$ pairs via gluon splitting, whereas the jets in $W+$ jets events consist of an approximately equal mixture of gluon and light-quark jets. These very simple qualitative arguments are borne out by a more quantitative calculation, as we will illustrate below.

The second way of estimating the $WQ\bar{Q}$ background (Method II) is based on an explicit calculation of the $WQ\bar{Q}$ process. Just as in the Wc case, uncertainties on the overall normalization of the $W+$ jets calculation are minimized by using as the theoretical input the fraction of $W+$ jets events that contain a $Q\bar{Q}$ pair, rather than the absolute rate prediction. The absolute background level is then estimated by multiplying this fraction by the number of observed $W+$ jets events and the tagging efficiencies for $Wc\bar{c}$ and $Wb\bar{b}$.

The $WQ\bar{Q}$ fraction is estimated using a combination of the HERWIG Monte Carlo event generator and the lowest order $WQ\bar{Q}$ matrix element (Fig. 52) calculation (Mangano, 1993). This calculation differs from the $W+$ jets calculation in that it includes all mass effects and is therefore free from collinear and infrared divergencies. Since the calculation does not include higher order terms, it cannot be used directly to estimate the $WQ\bar{Q}$ rate in events with more than two jets, which are the most relevant for the top search. Instead, the results of the exact calculation are compared to those of HERWIG, where the $Q\bar{Q}$ pairs are produced by gluon splitting from initial- and final-state parton evolution. The HERWIG results are found to be in good agreement with those of the $WQ\bar{Q}$ matrix element calculation. The gluon splitting process in HERWIG also provides a good description of the measured tagging rate in generic-jet events, giving further evidence for the validity of the HERWIG model. Thus, this model is used to predict the fraction of $WQ\bar{Q}$ events as a function of jet multiplicity. For the sample of $W+\geq 3$ jets, it is estimated that the fractions of W events containing a $b\bar{b}$ or $c\bar{c}$ pair are approximately 3% and 5% respectively. The systematic uncertainties associated with these predictions are clearly significant and are estimated to be at the level of 80%. The $WQ\bar{Q}$ background estimated with this method turns out to be approximately a factor of three lower than the conservative estimate made under the assumption that the heavy flavor content of jets in $W+$ jets events is the same as that of generic-jets.

To assess the impact of the $WQ\bar{Q}$ background on the top search, we re-examine the predicted rates of lepton + jets from $t\bar{t}$ and $W+$ jets. For example, from Fig. 42, the signal-to-background for a $W+$ 4 jets selection, with jet P_T threshold set at 15 GeV/c, is expected to vary from approximately 3/1 at M_{top} = 120 GeV/c^2 to approximately 1/3 at M_{top} = 200 GeV/c^2. With the fraction of $W+$ jets events containing a $Q\bar{Q}$ pair given above, the signal-to-background, ($t\bar{t}$ vs. $WQ\bar{Q}$) will be at least of the order of 7/1. Thus, provided the instrumental backgrounds can be adequately controlled, and enough luminosity is available to the experimenters, the top signal can be separated from the $W+$ jets background with b-tagging methods.

VI. EARLY SEARCHES FOR THE TOP QUARK

Experimental searches for the top quark began immediately following the discovery of the b-quark. In this Section we will review these searches up to approximately 1990.

A. Searches in e^+e^- collisions

In e^+e^- collisions, top quarks would be produced in pairs through e^+e^- annihilation into a photon or a Z. Since at leading order this is a purely electroweak process, the production cross-section can be accurately calculated. At center-of-mass energies well below the Z mass, where annihilation of the e^+e^- pair into a photon dominates, $t\bar{t}$ production would manifest itself as an increase by an amount $\delta\mathrm{R} \approx 3\mathrm{Q}_{top}^2 = 4/3$ in the ratio $\mathrm{R} = \sigma(e^+e^- \rightarrow \text{hadrons}) / \sigma(e^+e^- \rightarrow \mu^+\mu^-)$ well above the energy threshold for the production of a $t\bar{t}$ pair. This expected increase in R is largely independent of the top quark decay mode, as long as the top-quark decays into final states containing hadrons.

Between 1979 and 1984, measurements of R were performed at the PETRA e^+e^- collider in the center-of-mass energy range between 12 and 46.8 GeV (Barber *et al.*, 1979 and 1980; Berger *et al.*, 1979 and 1980; Bartel *et al.*, 1979a, 1979b, and 1981; Brandelik *et al.*, 1982; Adeva *et al.*, 1983a, 1983b, 1985, and 1986; Behrend *et al.*, 1984; Althoff *et al.*, 1984a and 1984b). The value of R was found to be consistent with Standard Model expectations without a top-quark contribution. Event topology studies gave no evidence for excesses of spherical, aplanar, or low thrust events that could be attributed to $t\bar{t}$ production. The measured rate of prompt muons was also found to be in agreement with expectations from models of c- and b-quark production and decay, and could not accommodate a contribution from semileptonic decays of top quarks. Existence of the top quark with mass below 23.3 GeV/c^2 was ruled out at the 95% confidence level (C.L.).

Similar searches were later performed at the TRISTAN collider, which reached a center-of-mass energy of 61.4 GeV (Yoshida *et al.*, 1987; Sagawa *et al.*, 1988; Adachi *et al.*, 1988; Igarashi *et al.*, 1988; K. Abe *et al.*, 1990). No evidence for top quark production was reported, resulting in a lower limit on the top mass of 30.2 GeV/c^2.

In 1989-90, the SLC and LEP e^+e^- colliders, with $\sqrt{s} \approx \mathrm{M}_z$ became operational. Studies of event topologies and measurements of the Z width were found to be inconsistent with a $Z \to t\bar{t}$ contribution, and resulted in lower limits on the top quark mass as high as 45.8 GeV/c^2 (Abrams *et al.*, 1989; Akrawi *et al.*, 1990a; Decamp *et al.*, 1990; Abreu *et al.*, 1990b and 1991; Adriani *et al.*, 1993).

B. Early searches in $p\bar{p}$ collisions assuming Standard Model top-quark decay

With the emergence in the 1980's of $p\bar{p}$ colliders, first at CERN and then at Fermilab, and with evidence from e^+e^- experiments pointing towards a very high mass for the top quark, focus in the search for top rapidly shifted to hadron colliders. The obvious advantage of hadron colliders for top physics is the high center of mass energy, which enables the exploration of higher mass regions. However, unlike in e^+e^- collisions, the large backgrounds make it impossible to directly search for the top quark in a model-independent way. It is necessary to concentrate on particular signatures, based for example on the Standard Model decay modes of the top quark discussed in the previous Section.

In this Section we will discuss searches for the top quark in $p\bar{p}$ collisions, assuming Standard Model top-quark decay, that were carried out in the mid to late 1980's at CERN and Fermilab. No evidence for top quark production was uncovered, leading to lower limits on the top quark mass as high as 91 GeV/c^2, at the 95% C.L.. These searches do not result directly in limits on the top mass, but rather in upper limits on the product of top production cross-section and branching ratio for top quark decay. To turn these limits into mass limits for the top quark, it is necessary to (i) assume that the top quark decays as $t \to Wb$, as prescribed by the Standard Model, and (ii) use theoretical expectations for the production cross-section. As discussed in Section IV, the main production mechanisms are $W \to t\bar{b}$ decays at S$p\bar{p}$S energies, and $t\bar{t}$ pair production at Tevatron energies. The expected cross-section for $p\bar{p} \to W \to t\bar{b}$ can be reliably predicted from direct measurements of $p\bar{p} \to W \to l\nu$; on the other hand, there are significant theoretical uncertainties on the predicted top-pair production cross-section as a function of the top mass, see Section IV, Figs. 21 and 22. Since these theoretical uncertainties are difficult to quantify, limits on M_{top} in the absence of a top signal in the data are placed based on the lower range of the calculation of the top production cross-section. This results in conservative 95% C.L. lower limits on M_{top}.

Initial results reported by the UA1 collaboration (Arnison *et al.*, 1984; Revol, 1985) at the CERN S$p\bar{p}$S collider ($\sqrt{s}$ = 630 GeV/c), seemed to be consistent with production of a top quark of mass 40 ± 10 GeV/c^2. These results were based on the observation of 12 isolated lepton + 2 jets events, with an expected background of approximately 3.5 events in an exposure with an integrated luminosity of 200 nb^{-1} (Revol, 1985). In these events, the invariant mass of the lepton, neutrino and one of the jets was found to cluster around a common value of approximately 40 GeV/c^2, while the invariant mass of the two jets, the lepton, and the neutrino was found to be consistent with the W mass. This is the expected signature for the process $p\bar{p} \to W \to t\bar{b}$, followed by $t \to bl\nu$. The excess of events over the background prediction was also consistent with the expected top production cross-section, providing further evidence for a top quark with $\mathrm{M}_{top} \approx 40$ GeV/c^2.

These first results were however not supported by a subsequent UA1 analysis (Albajar *et al.*, 1988), with a higher statistics data sample, as well as a more complete evaluation of the backgrounds. This analysis was based on samples of events with one isolated muon + ≥ 2 jets or one isolated electron + ≥ 1 jet. The integrated luminosity was 700 nb^{-1}. Given this integrated luminosity, and the expected top production rate, this search was sensitive to a top quark with $M_{top} < 55$ GeV/c^2. A maximum lepton-neutrino transverse mass requirement of 40 (45) GeV/c^2 was imposed in the muon (electron) sample to substantially reduce the $W \to l\nu$ background, while maintaining good efficiency for top quarks in the relevant mass range. No missing transverse energy ($\not{E}_T$) requirement was imposed, since for low top mass the probability for **both** the lepton and the neutrino in $t \to bl\nu$ to have high transverse momentum is low.

With no $\not{E}_T$ requirement, the backgrounds from fake leptons, Drell-Yan l^+l^- pairs, as well as $b\bar{b}$ and $c\bar{c}$ production are significant. The number of observed events was found to be fully consistent with the non-top background contribution only. Furthermore, it was shown that the event selection requirements resulted in background invariant mass distributions that were similar to those expected from top-quark production and decay (for $M_{top} \approx 40$ GeV/c^2). Thus, this property of the background accounted for the features of the invariant mass distributions observed in the previous analysis. Dilepton events were also studied, and their properties were found to be in agreement with expectations from semileptonic decays in $b\bar{b}$ and $c\bar{c}$ events.

An upper limit on the combined $W \to t\bar{b}$ and $t\bar{t}$ cross-sections was extracted from the background-subtracted lepton + jets event rates, as well as kinematic distributions such as those of jet E_T, $\not{E}_T$, and lepton isolation. At the time that these results were obtained, only a LO calculation for $p\bar{p} \to t\bar{t}$ was available. Using a conservative value for this cross-section the limit was inferred to be $M_{top} > 44$ GeV/c^2 at the 95% confidence level. A subsequent re-evaluation (Altarelli *et al.*, 1988), based on the NLO calculation of heavy-quark pair-production (Nason, Dawson, and Ellis, 1988) resulted in a slightly modified lower limit $M_{top} > 41$ GeV/c^2. This limit is obtained from the $t\bar{t}$ cross-section corresponding to the lower range of the theoretical prediction.

The lesson to be learned from the UA1 experience is that the reliability of background estimates is of paramount importance. Their first analysis did not include the J/Ψ, Υ, and Drell-Yan backgrounds, and the $b\bar{b}+c\bar{c}$ backgrounds were underestimated by a factor of four. The top signature at hadron colliders is complicated, and involves comparing the number of observed events and/or kinematic distributions with background expectations. If at all possible, dependences on uncertain theoretical models of background processes should be minimized.

More sensitive searches for the top quark were performed in the period 1988-89. At CERN, the new Antiproton Accumulator Complex (AAC) was commissioned, resulting in luminosities as high as 3 x 10^{30} cm^{-2} s^{-1} for the S$p\bar{p}$S. The UA1 electromagnetic calorimeter was removed to allow for a replacement based on Uranium-TMP (tetramethylpentane) technology. This new calorimeter was unfortunately not ready to be installed, resulting in the loss of electron identification in UA1. The UA2 detector at the CERN S$p\bar{p}$S was significantly upgraded, with improved calorimeter coverage, and enhanced electron detection capabilities. In the US, the first high-luminosity (up to 2 x 10^{30} cm^{-2} s^{-1}) run of the Tevatron Collider also started in 1988, with the CDF detector ready for data-taking.

The 1988-89 UA1 top search (Albajar *et al.*, 1990) was based on an integrated luminosity of 4.7 pb^{-1}, a factor of seven higher than had been previously available. Because of the missing EM calorimeter, only $\mu + \geq 2$ jets and $\mu\mu$ final states were considered. The μ + jets analysis was essentially an extension of the previous UA1 search (Albajar *et al.*, 1988), with the maximum transverse mass requirement raised to 60 GeV/c^2. For each event, a likelihood-like variable ($\mathcal{L}_1$) was defined to discriminate between top and background on an average basis. This likelihood was based on the $\not{E}_{\rm T}$, the isolation of the muon, and the opening angle between the muon and the highest E_T jet in the event.

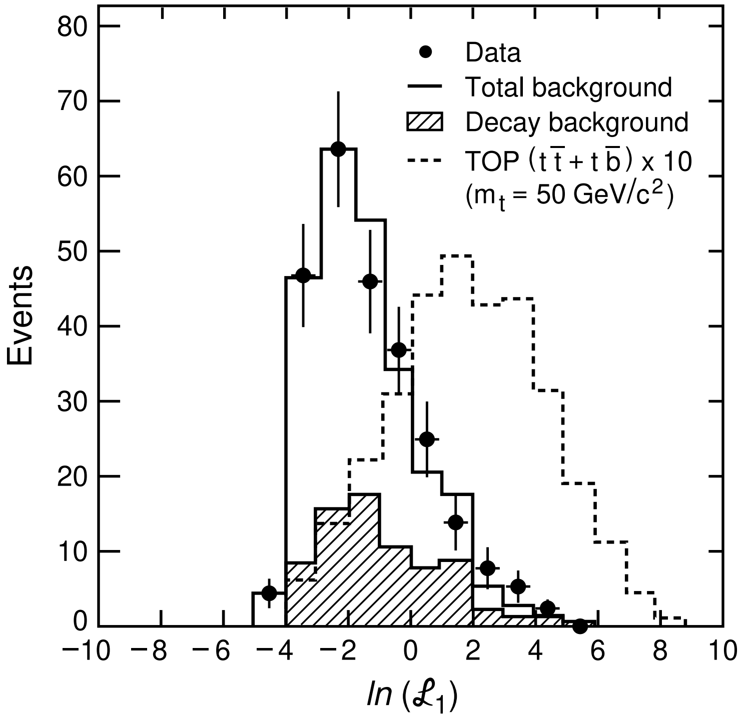

FIG. 55. The $\ln(\mathcal{L}_1)$ distribution compared with the expected background and top contributions. The shaded histogram is for the K and $\pi \to \mu\nu$ background. The other major background contribution is from $b\bar{b}$ and $c\bar{c}$ events. The expected top contribution, scaled up by a factor of 10, is shown in the dashed histogram. From the UA1 collaboration, Albajar *et al.*, 1990.

The $\mathcal{L}_1$ distributions of data, expected background, and expected signal, are shown in Fig. 55. The data are well-described by the background contribution only. Based on the number of observed events with $\ln(\mathcal{L}_1) > 4$, and the expected top production cross-section, the μ+ jets data from UA1 results in a lower limit on the mass of the top quark of 52 GeV/c^2 at the 95% confidence level.

A similar likelihood variable was defined for $\mu\mu$ events, based on the transverse momentum and isolation of the highest P_T muon, and the azimuthal opening angle between the two muons. Recall that at $\sqrt{s} = 0.63$ TeV for $M_{top} > 40$ GeV/c^2 the major source of top events is W decays, $W \to t\bar{b}$, see Section IV. Hence, the dilepton final state arises from semileptonic decays of both the t- and b-quarks, and the muon from $b \to c\mu\nu$ is not expected to be isolated. Studies of the likelihood distribution for $\mu\mu$ events also gave a null result.

Results from the $\mu +$ jets and the $\mu\mu$ data were combined with the lower statistics earlier UA1 results, yielding a lower limit on the top mass of 60 GeV/c^2 (95% C.L.).

A better limit on the top-quark mass was also obtained at the same time by the UA2 collaboration, based on an integrated luminosity of 7.5 pb^{-1} at the S$p\bar{p}$S (Akesson *et al.*, 1990). Without muon detection capabilities, the UA2 results were based entirely on the electron + $\geq$ 1 jet channel. The UA2 search strategy differed considerably from that of UA1, with a $\not\!\!E_{\mathrm{T}}$ > 15 GeV and an electron isolation requirement imposed in the event selection. As a result, backgrounds from $b\bar{b}$, $c\bar{c}$, and fake electrons were highly suppressed, and contributed only of order 10% to the data sample. The bulk of the background was due to $W \to e\nu +$ jets events. As was discussed in Section V.E.2, for M$_{top}$ < M$_W$+ M$_b$, the W in the decay $t \to Wb$ is virtual. The differences between the lepton-neutrino transverse mass distributions of real and virtual $W \to l\nu$ can then be exploited to separate a top signal from the background.

In Fig. 56 we show the transverse mass distribution for electron + jet + $\not\!\!E_{\mathrm{T}}$ events in UA2. No evidence for an excess of low transverse mass events was found, resulting in a lower limit of M$_{top}$ > 69 GeV/c^2.

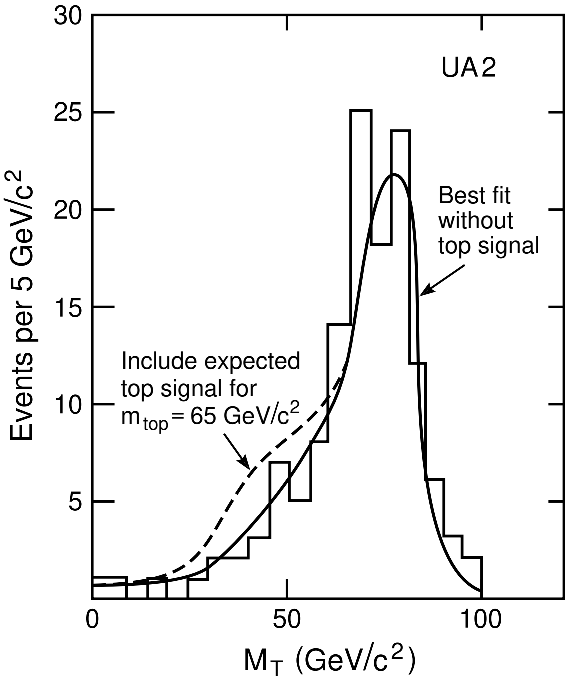

FIG. 56. The electron-neutrino transverse mass distribution in electron + jet + $\not\!\!E_{\mathrm{T}}$ events. The data are inconsistent with a top contribution. From the UA2 collaboration, Akesson *et al.*, 1990.

The first high statistics run of the Tevatron Collider also took place in 1988-89, with an integrated luminosity of 4 pb^{-1} recorded by the CDF collaboration. As was discussed in Section IV, at the center-of-mass energy of the Tevatron ($\sqrt{s}$ = 1800 GeV), top production in the relevant M$_{top}$ range is dominated by the $p\bar{p} \to t\bar{t}$ process. The CDF collaboration searched for top in both the lepton + jets (see Section V.E) and dilepton (see Section V.D) modes.

The CDF top search in the isolated electron + ≥ 2 jets channel (F. Abe *et al.*, 1990a and 1991a) was qualitatively similar to the UA2 search. An explicit $\not\!E_{\mathrm{T}}$ requirement was imposed, yielding a data sample containing $W \rightarrow e\nu$ + 2 jets events, with a small contamination from semileptonic b- and c-quark decays, as well as fake electrons. The resulting transverse mass distribution was found to be consistent with no top contribution, (see Fig. 57). The existence of a Standard Model top quark with 40 GeV/c^2 < M$_{top}$ < 77 GeV/c^2 was ruled out. (The limit was not extended below 40 GeV/c^2 because of poor acceptance at low top quark mass). Consistent results were also found in a subsequent study of μ+ jets events (Demortier, 1991).

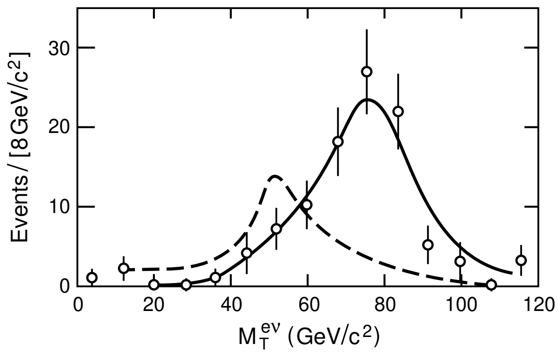

FIG. 57. The transverse mass distribution of electron + two or more jets + $\not\!E_{\mathrm{T}}$ events. From the CDF collaboration, (F. Abe *et al.*, 1990a). The solid and dashed lines represent expectations from the W + 2 jets and $t\bar{t}$ (M$_{top}$ = 70 GeV/c^2) Monte Carlo calculations.

Both the UA2 and CDF results were based on studies of the shape of the transverse mass distribution in lepton + jets events and were therefore independent of uncertainties in the theoretical predictions for the $p\bar{p} \rightarrow W+$ jets cross-section. Furthermore, the shape of the transverse mass distribution depends only weakly on the details of $W+$ jets production. It is sensitive mostly to the kinematics of the W decay, and the $\not\!E_{\mathrm{T}}$ resolution in the detector, and it is fairly insensitive to the transverse momentum of the W, see the discussion in Section V.E.2. Therefore, the influence of the theoretical modelling of the background was minimized in the CDF and UA2 lepton + jets top searches.

The CDF collaboration also searched for $t\bar{t}$ production in the dilepton channel. Initially, only the $e\mu$ channel was considered (F. Abe *et al.*, 1990b). As discussed in Section V.D, the $t\bar{t}$ dilepton signature consists in principle of two isolated high P$_T$ leptons, $\not\!E_{\mathrm{T}}$ and two jets. Since the backgrounds in this channel are small, in order to maximize the top acceptance, no $\not\!E_{\mathrm{T}}$, isolation, or jet requirements were imposed. One event was observed, with an expected background of 1.4 events, mostly from $Z \rightarrow \tau\tau$ followed by leptonic decays of both taus. An upper limit on the $t\bar{t}$ production cross-sections was then obtained based on the observation of one event, under the conservative assumption that this one event was due to $t\bar{t}$ production and decay. The mass region 28 < M$_{top}$ < 72 GeV/c^2 was excluded at the 95% C.L.

A subsequent CDF search (F. Abe *et al.*, 1992a) in the dilepton channel, based on the same integrated luminosity of 4 pb^{-1}, also included the ee and $\mu\mu$ channels, resulting in an increase in the top acceptance by a factor of two. As discussed in Section V.D, backgrounds in the ee and $\mu\mu$ channels are in general higher than in the $e\mu$ channel. $Z \rightarrow ee$ and

Experiment	Integ. luminosity	Mode	Mass limit (95% C.L.)	Ref.
UA1	5.4 pb^{-1}	μ + jets,	> 52 GeV/c^2	Albajar *et al.*, 1988
UA1	5.4 pb^{-1}	μ + jets, $\mu\mu$	> 60 GeV/c^2	Albajar *et al.*, 1988
UA2	7.5 pb^{-1}	e + jets	> 69 GeV/c^2	Akesson *et al.*, 1990
CDF	4 pb^{-1}	$e\mu$	> 72 GeV/c^2	F. Abe *et al.*, 1990b
CDF	4 pb^{-1}	e+ jets	> 77 GeV/c^2	F. Abe *et al.*, 1990a
CDF	4 pb^{-1}	dileptons $(ee, \mu\mu, e\mu)$	> 85 GeV/c^2	F. Abe *et al.*, 1992a
CDF	4 pb^{-1}	dileptons and l + jets +$b-$tag	> 91 GeV/c^2	F. Abe *et al.*, 1992a

TABLE VI. Summary of lower limits on the top quark mass from $p\bar{p}$ collisions, circa 1992. See text for details.

$Z \to \mu\mu$ decays were eliminated by an invariant mass cut, leaving a large number of events from off-shell Drell-Yan production of ee and $\mu\mu$ pairs. In order to control this background, additional requirements were imposed on the $\not{E}_T$ and the azimuthal opening angle between the two leptons.

No events consistent with $t\bar{t}$ were found in the ee and $\mu\mu$ channels. The resulting limit from the dilepton (ee + $\mu\mu$ + $e\mu$) channel was $M_{top} > 85$ GeV/c^2, at the 95% confidence level.

The CDF experiment also searched for top-quarks in the electron or muon + ≥ 2 jets channel, where the dominant $W+$ jets background was reduced by attempting to tag b-quarks through their semileptonic decay into muons, $b \to \mu$ or $b \to c \to \mu$ (F. Abe *et al.*, 1992a). No events consistent with the top hypothesis were found. Despite the high branching ratio for the lepton + jets mode, the acceptance in this search was approximately a factor of 3 smaller than that of the search in the dilepton channel for $M_{top} \sim 90$ GeV/c^2. The low acceptance was the consequence of the low ($\approx 4.5\%$) muon tagging efficiency for lepton + jets top events. This low tagging efficiency was due to (i) the semileptonic b-quark branching ratio, (ii) the limited ($|\eta| < 0.6$) muon coverage of the CDF detector as configured for the 1988-89 run, and (iii) the low transverse momentum of b-quarks in top decays for $M_{top} \sim 90$ GeV/c^2. Combining results from this search and the dilepton search, resulted in a 95% C.L. lower limit on the top quark of 91 GeV/c^2, (see Fig. 58). This limit was extracted using the NLO calculation of the $t\bar{t}$ cross-section (Ellis, 1991). The 91 GeV/c^2 limit corresponds to the point where the cross-section limit curve crosses the lower (i.e. more pessimistic) bound of the theoretical prediction. Using a more up-to-date calculation of $\sigma(t\bar{t})$ (Laenen, Smith, and van Neerven, 1994), would result in a limit of 95 GeV/c^2.

The lower limits on the top mass from the UA1, UA2, and CDF experiments are summarized in Table VI. With the top quark being so massive, hopes to observe the top quark at the CERN S$p\bar{p}$S were abandoned, because of the small top production cross-section at $\sqrt{s} = 630$, (see Fig. 22). In Section VIII we will discuss the most recent, higher statistics, searches for the top quark at the Tevatron Collider, which finally resulted in the discovery of the top quark.

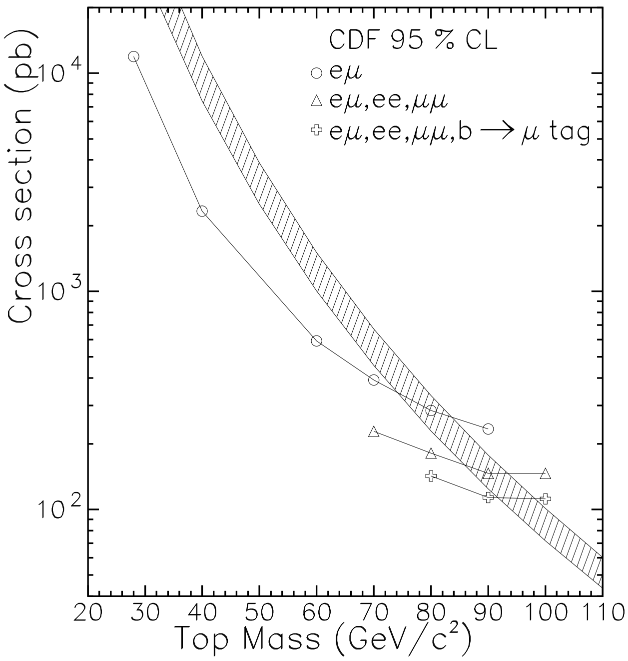

FIG. 58. The 95% C.L. upper limits on the $t\bar{t}$ cross-section from F. Abe *et al.*, 1992a. Circles : $e\mu$ channel only. Triangles : dilepton channel ($e\mu$, ee, and $\mu\mu$). Crosses : dilepton channel + lepton + jets with a $b \to \mu$ tag. The band represents the NLO theoretical prediction for the $t\bar{t}$ cross-section from Ellis, 1991. The integrated luminosity was 4 pb^{-1}. The cross-section limits are a function of the top mass because the $t\bar{t}$ acceptance depends on the top mass.

C. Searches for non-Standard Model top quark decay modes

The lower limits on M_{top} from $p\bar{p}$ collisions discussed in Section VI.B are not valid if the top quark does not decay as $t \to Wb$. If $\mathrm{M}_{top}+ \mathrm{M}_b < \mathrm{M}_W$, the decay $W \to t\bar{b}$ is possible and contributes to the width of the W boson, $\Gamma(W)$.

The width of the W is difficult to measure directly since the mass signature of the W is a Jacobian and not a Breit-Wigner (see Fig. 43), and because the $\not{E}_{\mathrm{T}}$ resolution is much larger than the natural width of the W. However, constraints on the top quark mass independent of decay mode can be obtained from measurements of the leptonic W branching ratio $Br(W \to l\nu) = \Gamma(W \to l\nu)/\Gamma(W)$, based on theoretical expectations for $\Gamma(W \to l\nu)$. At lowest order the branching ratio varies between $Br(W \to l\nu) = 1/9$ for $\mathrm{M}_W < \mathrm{M}_{top}+ \mathrm{M}_b$ and $Br(W \to l\nu) = 1/12$ for for very light M_{top}. Experimentally, a value for this branching ratio can be extracted from measurements of the ratio

$$R = \frac{\sigma(p\bar{p} \to W) \;\; Br(W \to l\nu)}{\sigma(p\bar{p} \to Z) \;\; Br(Z \to l^+l^-)}$$

(Cabibbo, 1983; Halzen and Marsula, 1983; Hikasa, 1984; Deshpande *et al.*, 1985; Martin, Roberts, and Stirling, 1987; Berger *et al.*, 1989). The value of the Z leptonic branching ratio is taken from the very precise measurements in e^+e^- annhilations at LEP and SLC (Montanet *et al.*, 1994). The values of $\sigma(p\bar{p} \to W)$ and $\sigma(p\bar{p} \to Z)$ can be calculated in QCD; note that theoretical uncertainties in these calculations largely cancel in the ratio, and the uncertainty in $\sigma(p\bar{p} \to W)/\sigma(p\bar{p} \to Z)$ is only of order 1%. (Martin, Roberts, and Stirling, 1989; Hamberg, van Neerven and Matsuura, 1991; van Neerven and Zijlstra, 1992).

Early measurements of this ratio from the $Sp\bar{p}S$ were found to be more consistent with a small top quark mass (Albajar *et al.*, 1987; Ansari *et al.*, 1987). These results were used by several authors to set upper limits on the top quark mass, e.g. $M_{top} < 63$ GeV/c^2 at 90% C.L. (Martin, Roberts, and Stirling, 1987); $M_{top} < 60$ GeV/c^2 at 95% C.L. (Halzen, Kim and Willenbrock, 1988); $M_{top} < 70 \pm 5$ GeV/c^2 at 90% C.L. (Colas, Denegri and Stubenrauch, 1988). However, subsequent higher statistics studies at both the $Sp\bar{p}S$ (Albajar *et al.*, 1991a; Alitti *et al.*, 1992b) and the Tevatron (F. Abe *et al.*, 1990c, 1992c, 1994d; Abachi *et al.*, 1995e), found results consistent with expectations for a high top quark mass. A lower limit $M_{top} > 65$ GeV/c^2 at 95% C.L. can be extracted from the world average value of $Br(W \to l\nu)$, (see Fig. 59).

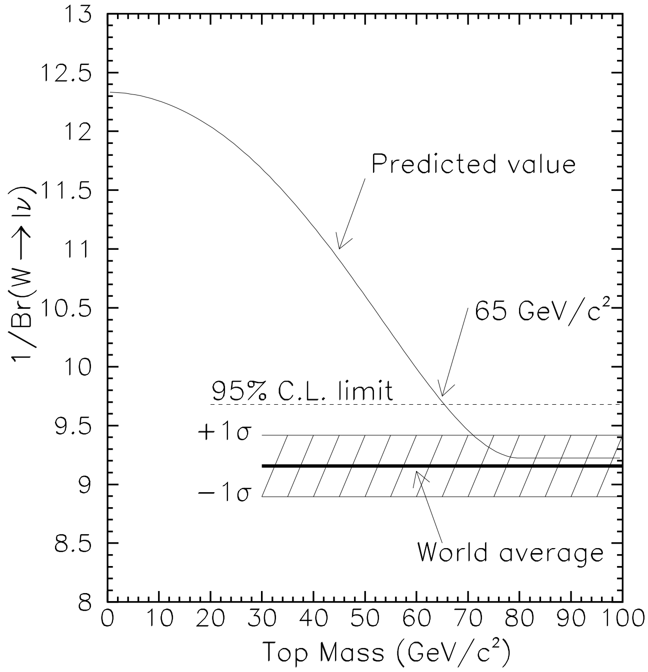

FIG. 59. World average value for the inverse $W \to l\nu$ branching ratio (Abachi *et al.*, 1995e), compared with Standard Model expectations as a function of the top quark mass. Also shown is the 95% lower limit on M_{top}, independent of top quark decay mode, which can be extracted from the measurement.

Direct searches for top quarks decaying into final states different from Wb have also been carried out at $p\bar{p}$ colliders. The decay $t \to H^+b$ is allowed in several models in which the Higgs sector is extended to include charged Higgs scalars (H^+). This includes non-minimal Standard Models, such as supersymmetry (Gunion *et al.*, 1990). In the simplest version of these models, there are two Higgs doublets, and the decay $t \to H^+b$ dominates for $M_{top} <$ $M_W +$ M_b. At higher top masses, both $t \to H^+b$ and $t \to Wb$ are allowed. The branching ratios for the two modes are functions of M_{top}, M_{H^+}, and a theoretically unconstrained parameter tanβ, which is the ratio of vacuum expectation values for the two Higgs doublets. The charged Higgs scalar from top decay would then decay into the heaviest lepton or quark pair ($\tau\nu$ or $c\bar{s}$), with branching fractions which also depend on the value of tanβ (Glashow and Jenkins, 1987; Barger, Hewett, and Phillips, 1990; Dress and Roy, 1991).

Searches for $t \rightarrow H^+b$, $H^+ \rightarrow \tau\nu$ based on the identification of hadronic tau decays have been carried out by the UA1 (Albajar *et al.*, 1991b), UA2 (Alitti *et al.*, 1992c), and CDF (F. Abe *et al.*, 1994c) collaborations. No evidence for this process was found, and limits were placed as a function of M_{top}, M_{H+}, and the $H^+ \rightarrow \tau\nu$ branching ratio. The most stringent limits are the result of a higher statistics analysis from the CDF collaboration (F. Abe *et al.*, 1994e) based on the $\tau \rightarrow e$ or μ signature, (see Fig. 60).

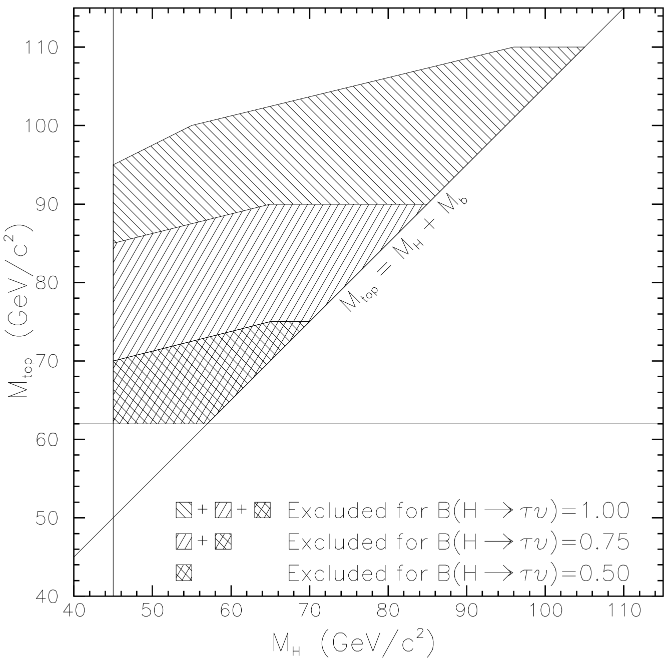

FIG. 60. Regions of the (M_{top} $-M_{H+}$) plane excluded at 95% C.L. for different values of the branching ratio for $H^+ \rightarrow \tau\nu$. From the CDF collaboration, F. Abe *et al.*, 1994e. The vertical line reflects the lower limit $M_{H+} > 45$ GeV/c^2 from the LEP experiments, (Buskulic *et al.*, 1992; Abreu *et al.*, 1990a; Adriani *et al.*, 1992; Akrawi *et al.*, 1990b). The horizontal line reflects the lower limit $M_{top} > 62$ GeV/c^2 from F. Abe *et al.*, 1994d, based on $Br(W \rightarrow l\nu)$. The integrated luminosity is 19 pb^{-1}.

VII. THE FERMILAB PROTON ANTI-PROTON COLLIDER

The Fermilab $p\bar{p}$ Collider in Batavia, Illinois consists of seven accelerating structures, see Fig. 61. It is the highest energy particle accelerator in the world, with a center-of-mass energy of 1800 GeV (Fermilab, 1984).

A. Linear accelerators and synchrotrons

Negatively charged hydrogen ions (H^-) are initially accelerated by a Cockroft-Walton pre-accelerator to 750 keV. These ions are then accelerated in a 145 meter linear accelerator to 400 MeV. They are stripped of their two electrons as they are injected into the first proton synchrotron called the *Booster*. The Booster is a ring of 150 meter diameter, where 18 accelerating cavities are used to accelerate the protons to 8 GeV. The protons are then extracted and injected into the *Main Ring*, which is the original 2 kilometer diameter Fermilab proton synchrotron comissioned in 1972.

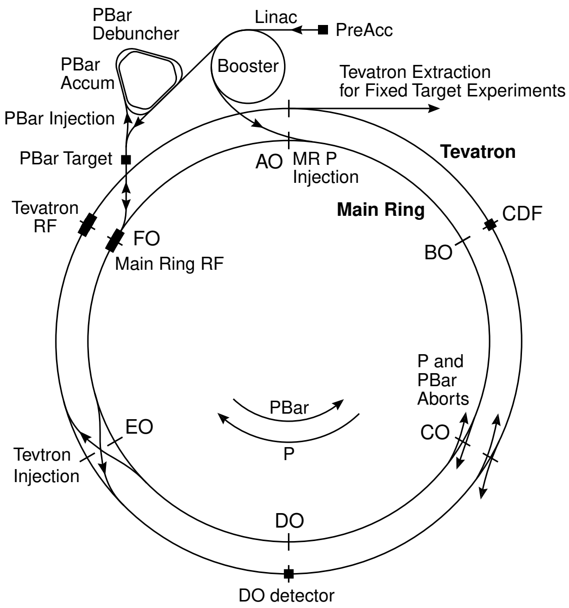

FIG. 61. The Fermilab accelerator complex. From Thompson, 1994.

The Main Ring was built with conventional electromagnets with a maximum dipole bending field of .65 Tesla, with 18 accelerating cavities operating at about 53 MHz, giving a boost of 2.5 MeV per turn. The Main Ring has accelerated protons up to 500 GeV. It is now routinely used to accelerate protons to 120-150 GeV which are then injected into the final synchrotron, the *Tevatron*, or into the anti-proton cooling ring. The Tevatron built in 1983 uses superconducting magnets to bend and focus the beams, and is situated a meter below the Main Ring. The dipoles have a maximum dipole bending field of 4.4 Tesla and the focussing quadrupoles have a maximum field gradient of 67 Tesla/m. With 8 RF accelerating cavities the Tevatron gives the protons a boost of 1 MeV per turn and can accelerate the protons up to 900 GeV with an energy resolution of $\pm$ 0.9 GeV.

B. Anti-proton source

As was mentioned above, the Main Ring also acts as an injector to the $\bar{p}$ source (Church and Marriner, 1993). The protons are extracted from the Main Ring at 120 Gev and delivered to a target where anti-protons are produced with peak momentum of 8 GeV. The $\bar{p}$'s are then focussed in a lithium lens and fed into the *Debuncher*, which is a ring with a circumference of 500 meters. The $\bar{p}$ bunches are debunched, by turning the narrow time spread of the bunch and large momentum spread into a large time spread and a narrow momentum spread. After this bunch rotation, the $\bar{p}$'s are stochastically cooled (van der Meer, 1972), further reducing the phase space of the beam. The beam is then transferred to the *Accumulator*, added to the anti-protons already stored there using a process called stochastic stacking. When enough $\bar{p}$'s have been accumulated to make an intense beam, the beam is extracted and injected back into the Main Ring, where it is then accelerated and injected into the Tevatron.

During the period when the top data was collected, the accelerator operated with 6 bunches of protons and 6 bunches of anti-protons circulating in the machine. It takes approximately 2.5 hours of shining protons on the $\bar{p}$ source target every 2.4 seconds in order to accumulate enough $\bar{p}$'s to ensure a reasonable luminosity for $p\bar{p}$ collision. To optimize collider livetime, this process of creating and stacking the anti-protons took place during collider operation. This meant that there was often beam in the Main Ring while the collider experiments (CDF and D0) were taking data. The halo from this beam interacted with the walls of the accelerator and sprayed particles into the two collider detectors, depositing large amounts of energy in the calorimeters. In the case of CDF, the Main Ring was diverted via a dogleg up above the detector and shielded by a steel structure approximately one meter thick. Nevertheless, occasionally extra energy was deposited in the calorimeters. These events were rejected offline. The D0 experiment had no such dogleg or beam diversion and consequently the Main Ring ran straight through the D0 detector, approximately 2.5 meters above the Tevatron beampipe. The D0 collaboration was forced to turn off data acquisition while the Main Ring beam was passing through their detector, resulting in a 15% livetime loss.

C. Collider

The p and $\bar{p}$ bunches are approximately 50 cm in length due to the RF frequency of the accelerator. This bunch length determines the long luminous region at the interaction points, which is roughly Gaussian and has a sigma of approximately 30 cm. The length of the luminous region has many limiting features in terms of triggering and solid angle coverage by the detectors. For instance, as will be discussed later in this review, the silicon vertex detector in the CDF experiment was 50 cm long and thus, due to the size of the luminous region, had a limited acceptance of roughly 60% for bottom quarks from top quark decays. Furthermore, the measurements of transverse energies at the trigger level was smeared by the lack of knowledge of the event-by-event interaction position.

Accelerator radius	1000 m
Maximum beam energy	900 GeV
Injection energy	150 GeV
Peak luminosity	2 x 10^{31} cm^{-2} s^{-1}
Number of bunches	$6p, 6\bar{p}$
Intensity per bunch	$\approx 10^{11}p$, 5 x $10^{10}\bar{p}$
Crossing angle	0^o
Bunch length (1 σ)	50 cm
Transverse beam radius (1 σ)	$\approx$ 25 μm
Energy spread	0.15 x 10^{-3} GeV
RF frequency	53 MHz
$\bar{p}$ stacking rate	$\approx$3.5 x 10^{10}/hour
Beam crossing frequency	290 kHz
Period between crossings	3.5 μs

TABLE VII. Parameters of the Fermilab Tevatron Collider.

The Tevatron Collider complex was first commissioned with a short run in 1985. The first high-luminosity run took place in 1988-89, at which time only the CDF detector was ready for data-taking. The peak luminosity for that run was approximately 2 x 10^{30} cm^{-2}sec^{-1}, a factor of two higher than the initial design. The second set of high luminosity collider runs, Run Ia and Run Ib, begun in 1992 with data taken by both the D0 and CDF detectors. During these runs, the peak luminosity was 2 x 10^{31} cm^{-2}sec^{-1}, while the average luminosity was about 1.4 x 10^{31} cm^{-2}sec^{-1}. The lifetime of the beams in the Collider and the $\bar{p}$ stacking rate was such that new protons and anti-protons were injected into the Collider once a day. Table VII lists the relevant parameters of the Collider.

VIII. DISCOVERY OF THE TOP QUARK

In this Section we review the recent results that finally led to the establishment of the existence of the top quark. The discovery of the top quark was made possible by the remarkable success of the Tevatron Collider project, see Section VII. These results come from the two collider experiments (CDF and D0) at Fermilab's Tevatron. They are based on data from the 1992-93 (Run Ia) and 1994-1995 (Run Ib) runs of the collider. Analysis of data from the remainder of Run Ib was in progress at the time that this review was being written. Preliminary results from both CDF and D0 are fully consistent with those from the earlier data sets.

The data sets that were used to discover the top quark were collected during Run Ia and the first half of Run Ib. The total integrated luminosities were 67 pb^{-1} for CDF, and between 44 and 56 pb^{-1}, depending on top decay mode, for D0. The difference in integrated luminosities between the two experiments is due mostly to the fact that the Main Ring accelerator at Fermilab which operates asynchronously from the Tevatron, runs through the D0 calorimeter, see Section VII. Data taking in the D0 experiment must be disabled whenever a Main Ring proton bunch crosses the detector.

Given the $t\bar{t}$ production cross-section at the Tevatron (see Section IV), the number of $t\bar{t}$ pairs produced in an exposure of 67 pb^{-1} is expected to be between approximately 6800 (for M_{top} = 100 GeV/c^2) and 150 (for M_{top} = 200 GeV/c^2). This is a small number of events, especially in light of the fact that not all the the possible $t\bar{t}$ decay channels can be exploited, see the discussion in Section V. Thus, the high luminosity delivered by the Tevatron was crucial in enabling the experimenters to isolate the very rare top signal.

Both the CDF and D0 top searches assumed Standard Model decay ($t \to Wb$) of the top quark, and were based on the $t\bar{t}$ dilepton and lepton + jets signatures discussed in Section V. In all cases, the number of observed events, after a selection procedure designed to maximize the acceptance to top quarks, was compared with the number of expected events from non-$t\bar{t}$ sources. An excess of events over the background prediction then constitutes evidence for the top quark.

At the beginning of Run Ia, the best lower limit on the mass of the top quark was 91 GeV/c^2, from the 1989 CDF top search, see Section VI. The initial top selection criteria for both CDF and D0 were optimized for detection of a low mass ($M_{top} \approx$ 120 GeV/c^2) top quark. A lower limit of $M_{top} >$ 131 GeV/c^2 at the 95 % C.L. was established by D0 from the Run Ia data with an integrated luminosity of 13.5 pb^{-1} (Abachi *et al.*, 1994).

Initial evidence for the top quark was reported by the CDF collaboration (F. Abe *et al.*, 1994a) based on analysis of the Run Ia data set only, which had an integrated luminosity of 19.3 pb^{-1}. The excess in the number of top candidate events over the background prediction was 2.8 standard deviations. Additional kinematic features of the data, such as a reconstructed mass peak, also supported the $t\bar{t}$ hypothesis. However, these results were not deemed sufficient to unambiguously establish the existence of the top quark. Following the publication of a lower limit on M_{top}, the D0 requirements were reoptimized, i.e. tightened, for higher top masses. With the optimized requirements, a statistically not very significant excess of events (1.9 standard deviations) was also found in the Run Ia D0 data (Abachi *et al.*, 1995a and 1995d). With the addition of the data from the first half of Run Ib, a statistically convincing excess of events emerged from the analyses of the data sets from both collaborations (F. Abe *et al.*, 1995a; Abachi *et al.*, 1995b).

The CDF and D0 searches for $t\bar{t}$ in the dilepton channel were similar and are discussed in Section VIII.A. On the other hand, the search strategies in the lepton + jets channel were quite different. At the beginning of Run Ia, a silicon vertex detector was installed at CDF (Amidei *et al.*, 1994). Given the excellent b-tagging capabilities of this device (see Section V.E.4), b-tagging was used to separate the top signal in the lepton + jets channel from the $W+$ jets background. Both vertex tagging and lepton tagging ($b \to e$ as well as $b \to \mu$) were used in CDF. In contrast, a large fraction of the top sensitivity in this channel for the D0 experiment came from kinematic separation of $t\bar{t}$ and $W+$ jets, although lepton tagging ($b \to \mu$ only) was also employed. Analyses of the kinematic properties of lepton + jets events were also performed on the CDF data (F. Abe *et al.*, 1994a, 1995b, and 1995c). Excesses of top-like events were also seen in these CDF studies, and were used to confirm the results of the b-tagging observations.

In the remainder of this Section, we will describe in some detail the results from the CDF and D0 top searches. Dilepton searches will be reviewed in Section VIII.A, followed by a summary of the searches in the lepton + jets + b-tag channel in Section VIII.B, and of kinematic separation of $t\bar{t}$ and $W+$ jets in Section VIII.C. The results from the two experiments will then be summarized in Section VIII.D, and their measurements of the $p\bar{p} \to t\bar{t}$ cross-section will be presented in Section VIII.E.

Before beginning the discussion of the CDF and D0 results, we wish to point out a difference in when the measured jet energies are corrected back to the parent parton momenta in CDF and D0. In all D0 analyses, correction to the measured jet energies are made prior to the selection of the sample. (The jet energy correction procedure will be discussed extensively in Section IX.A.3). For most CDF analyses, the measured jet energies are not corrected at the event sample selection stage, or in the following analysis. Corrections are only applied when the measurement of the quark or gluon energy is needed, for example in the measurement of the top mass, see Section IX. Unfortunately, this makes it somewhat difficult to compare results from the two experiments. For the jet energies relevant to the top search (15 GeV $\lesssim$ E_T $\lesssim$ 150 GeV) the multiplicative correction factor for a CDF jet energy cluster is of order 1.5.

A. Dilepton analysis results from CDF and D0

The searches for top quarks performed in the dilepton channel by D0 and CDF are similar. We have discussed the dilepton analysis approach at a general level in Section V.D. What follows are the results of these two analyses. The main difference in analysis strategy between the two experiments is due to the fact that CDF has momentum determination from charged particle tracking in the central region whereas D0 does not, and that D0 imposes more stringent requirements on the transverse energies of the jets.

	Leptons		Jets			
Channel	E_T(e)	$P_T(\mu)$	$N_{\rm jet}$	E_T	$\not{E}_T$	H_T
$e\mu$ + jets	$\geq$ 15 GeV	$\geq$ 12 GeV/c	≥ 2	$\geq$ 15 GeV	$\geq$ 20 GeV	$\geq$ 120 GeV
ee + jets	$\geq$ 20 GeV	-	≥ 2	$\geq$ 15 GeV	$\geq$ 25 GeV	$\geq$ 120 GeV
$\mu\mu$ + jets	-	$\geq$ 15 GeV/c	≥ 2	$\geq$ 15 GeV	-	$\geq$ 100 GeV

TABLE VIII. A partial summary of selection criteria for $t\bar{t} \to$ dileptons in D0. Jets must have $|\eta| < 2.5$ and their energies are corrected. The lepton pseudorapidity coverages are $|\eta| < 2.5$ for electrons, $|\eta| < 1.7$ for muons in Run Ia, and $|\eta| < 1.0$ for muons in Run Ib. The loss of muon coverage is due to ageing of the forward muon chambers. The H_T requirement is discussed in the text.

Both analyses require two high P_T leptons, at least two jets and in most cases, high $\not{E}_T$. The exceptional case is the D0 search for decays in the $\mu\mu$ channel, where the $\not{E}_T$ requirement is removed. The resolution of the D0 muon momentum measurement is limited to of order 20% by multiple scattering in the toroids (see Table IV), and therefore in the $\mu\mu$ channel the measurement of the $\not{E}_T$ is poor and is not used in the D0 analysis. The major backgrounds to the top quark signature in the dilepton channel are due to events in which jets fake leptons, $Z \to ee/\mu\mu/\tau\tau$, Drell-Yan lepton pair production, WW and $b\bar{b}$ production. These backgrounds are reduced dramatically by the requirements listed in Table VIII and Table IX.

Channel	Leptons		Jets		$\not{E}_T$	$\Delta\phi(\not{E}_T$,lepton or jet$) > 20^o$
	E_T(e)	$P_T(\mu)$	N_{jet}	E_T		
$e\mu$ + jets	$\geq$ 20 GeV	$\geq$ 20 GeV/c	≥ 2	$\geq$ 10 GeV	$\geq$ 25 GeV	$\rightarrow \not{E}_T \geq 50$
ee + jets	$\geq$ 20 GeV	-	≥ 2	$\geq$ 10 GeV	$\geq$ 25 GeV	$\rightarrow \not{E}_T \geq 50$
$\mu\mu$ + jets	-	$\geq$ 20 GeV/c	≥ 2	$\geq$ 10 GeV	$\geq$ 25 GeV	$\rightarrow \not{E}_T \geq 50$

TABLE IX. A partial summary of selection criteria for $t\bar{t} \rightarrow$ dileptons in CDF. Jets must have $|\eta| < 2.5$ and their energies are not corrected. The lepton pseudorapidity coverage is $|\eta| < 1.0$. The $\not{E}_T$ requirement is tightened when the missing transverse energy vector is collinear with either a lepton or a jet. See the discussion in the text.

In particular, as discussed in Section V.D, asking for the presence of two jets in the event is a very powerful discriminator between signal and all sources of background.

There are two other differences in the kinematic requirements applied by CDF and D0. In the D0 analysis, there is a requirement on H_T, defined as $H_T \equiv \Sigma_{jets}(E_T) + E_T^e$ which is the scalar sum of all jet transverse energies plus the highest transverse energy electron in the event, if there is one. This is a kinematic variable that attempts to discriminate between the top signal and background, by exploiting the difference between the total transverse energy of the jets in top and background events. In Fig. 62 we show Monte Carlo predictions of H_T for the principal backgrounds and for $t\bar{t}$ events with $M_{top} = 200$ GeV/c^2.

For the CDF analysis, in events where the $\not{E}_T$ is nearly collinear with the P_T of the leptons or jets, the $\not{E}_T$ requirement is tightened. As we will show below, this procedure is somewhat effective at suppressing a number of background sources. We will now discuss the dilepton CDF and D0 results, starting with the background sources, and the specific CDF and D0 selection requirements designed to discriminate against them.

1. $Z \rightarrow ee/\mu\mu$ background

Z decays constitute an important background to the $t\bar{t}$ signal in the dilepton channel. Following the $E_T(e)$, $P_T(\mu)$ and N_{jet} requirements listed in Table VIII and Table IX there is still a substantial background from $Z + \geq 2$ jets, in which the Z decays to e^+e^- or $\mu^+\mu^-$. Since Z decays to charged leptons do not produce any neutrinos, no $\not{E}_T$ is expected in these events. Therefore, requiring large $\not{E}_T$ eliminates these backgrounds completely, except for the effects of mismeasurements of the missing transverse energy in the detector.

To eliminate the $Z \rightarrow ll$ background, e^+e^- and $\mu^+\mu^-$ events with dilepton invariant mass between 75 GeV/c^2 and 105 GeV/c^2 are rejected in the CDF top search. This requirement is expected to be approximately 75% efficient, roughly independent of top mass, for dileptons (e^+e^- and $\mu^+\mu^-$) from $t\bar{t}$ decays. In the D0 analysis, the requirements used to discriminate against the Z background differ in the e^+e^- and $\mu^+\mu^-$ channels because the resolution on the lepton energy/momentum measurement is so much better for electrons than it is for muons. In the e^+e^- channel, if the invariant mass (M_{ee}) of the pair is consistent with the Z mass (79 GeV/c$^2 \leq M_{ee} \leq 103$ GeV/c^2), the missing transverse energy requirement is tightened to $\not{E}_T \geq 40$ GeV. Note that this is in contrast to the CDF approach of rejecting any event that may be consistent with Z decays, regardless of the size of the missing transverse energy in

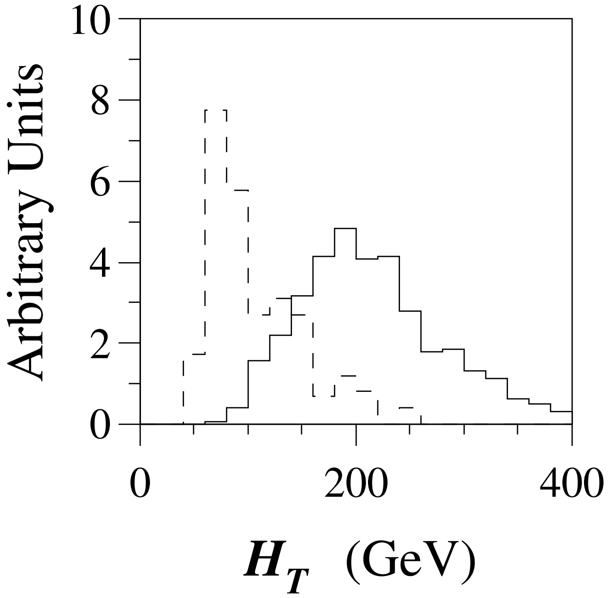

FIG. 62. D0 Monte Carlo predictions of the variable H_T for dilepton decays of a 200 GeV/c^2 top quark (solid) and principal dilepton backgrounds (dashed). From Abachi *et al.*, 1995b.

the event. As was discussed earlier, no $\not\!\!E_T$ information is used by D0 in the $\mu^+\mu^-$ channel. Z decays into muons are then rejected on the basis of an overall kinematic likelihood fit to the $Z \to \mu^+\mu^-$ hypothesis.

Since the Monte Carlo simulation is unlikely to correctly model the tails of the $\not\!\!E_T$ resolution, the D0 collaboration relies on multijet data to estimate the remaining $Z \to ee+$ jets background after the $\not\!\!E_T$ requirement. As a result of $\not\!\!E_T$ studies in the multijet sample, the fraction of $Z \to ee$ events with $\not\!\!E_T > 40$ GeV is estimated to be less than 2 x 10^{-4} (Abachi *et al.*, 1995d). The CDF requirement is more conservative and loses acceptance in return for certainty that there will be no Z decays in the top candidate sample. In Fig. 63 we show the distribution of the invariant mass of the electron-positron pair versus the $\not\!\!E_T$ for D0 events. Expectations for $t\bar{t}$ are displayed in Fig. 64.

It is difficult to compare directly the $\not\!\!E_T$ resolutions of CDF and D0. The parametrizations of the $\not\!\!E_T$ resolutions in the two experiments do not have the same functional form. The CDF resolution grows linearly with $\sqrt{\Sigma E_T}$ whereas the D0 resolution appears to grow linearly with ΣE_T, see Table V. The tails of the distribution in CDF are dominated by cracks in the calorimeter while the D0 detector design minimized cracks. The radioactive noise from the uranium plates in the D0 calorimeter adds of order 25 GeV per event to the total energy making difficult a direct comparison of the resolution at a particular ΣE_T.

2. $Z \to \tau\tau$ background

$Z \to \tau\tau$, followed by leptonic decays of both taus, is a very important background source. These events cannot be eliminated by an invariant mass cut, due to the presence of

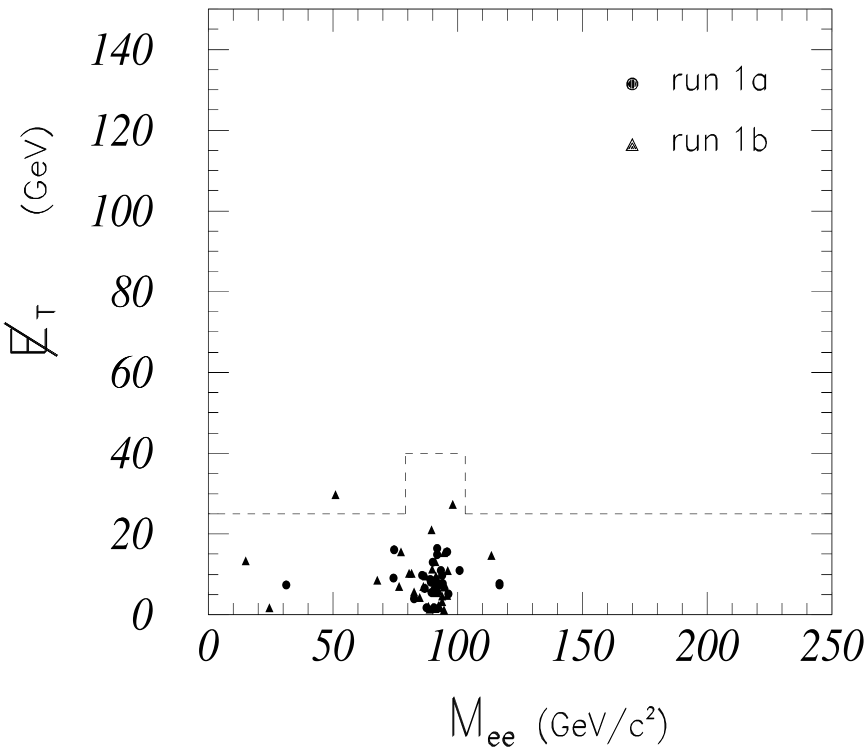

FIG. 63. Dielectron mass versus missing transverse energy in $ee+$ 2 jet events from D0 (Grannis, 1995). The integrated luminosity is 55.7 pb^{-1}. Also shown is the D0 $\not{E}_T$ requirement in the dielectron channel.

unmeasured neutrinos from $\tau \to l\nu\nu$. Furthermore, these neutrinos can give rise to $\not{E}_T$ in the event. The requirements on jet multiplicity, high E_T or P_T leptons, and high $\not{E}_T$ are all effective at reducing the background, see the discussion in Section V.D, and also Fig. 38. In Fig. 65 we show the $\not{E}_T$ versus dilepton mass for leptons from $Z \to \tau\tau$ decays from the ISAJET Monte Carlo. This clearly indicates that the background is not eradicated by the $\not{E}_T$ requirement alone.

In the decay of a high momentum τ, the decay products are highly collimated, due to the small mass of the τ lepton. As a result, in these events the $\not{E}_T$ will often point in the direction of one of the two leptons in the transverse plane. Therefore, in the CDF analysis the $\not{E}_T$ requirement is tightened to $\not{E}_T \geq 50$ GeV for events in which the azimuthal angle ($\phi_{\not{E}_T}$) of the $\not{E}_T$ vector is within 20° of the azimuthal angle (ϕ_{lepton}) of either of the two leptons, (see Fig. 66).

There is no such $\Delta\phi$ requirement for D0, see Table VIII. However the requirement made on H_T, see Table VIII, has a rejection power of approximately 2.5 for $Z \to \tau\tau+$ two or more jets.

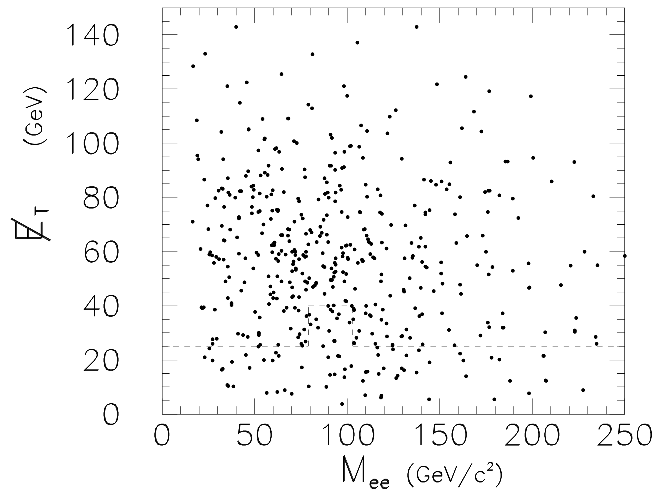

FIG. 64. Dielectron mass versus missing transverse energy in $t\bar{t} \rightarrow ee+$ 2 jets events from the D0 Monte Carlo (Grannis, 1995). Also shown is the D0 $\not\!\!E_T$ requirement in the dielectron channel.

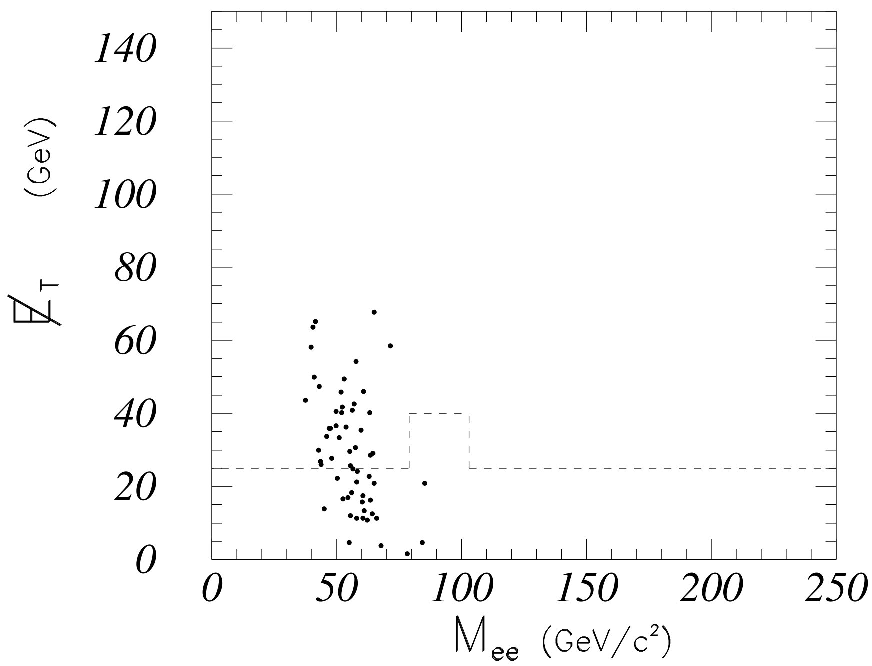

FIG. 65. Missing transverse energy versus dilepton mass for $Z \rightarrow \tau\tau + 2$ jets Monte Carlo events. From the D0 collaboration, Grannis, 1995. Also shown is the D0 $\not\!\!E_T$ requirement in the dielectron channel.

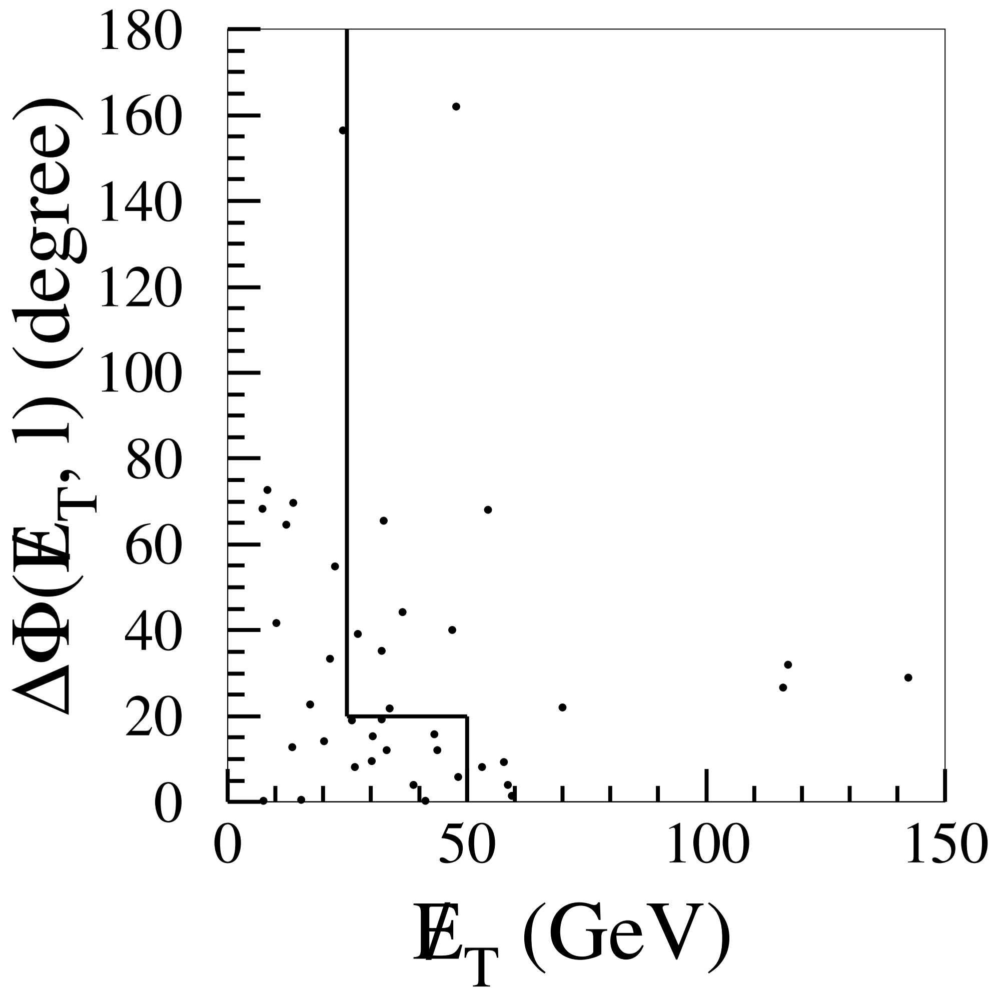

FIG. 66. CDF Monte Carlo distribution of the azimuthal angle between the $\not{E}_T$ and the closest lepton as a function of $\not{E}_T$ in $Z \to \tau\tau$ events with two jets. Also shown is the boundary of the CDF $\not{E}_T$ requirement. From the CDF collaboration, F. Abe *et al.*, 1994a.

3. Drell-Yan Background

Continuum Drell-Yan production of lepton pairs accompanied by two jets is a background not addressed by the Z mass requirement. In the CDF analysis, the $\Delta\phi$ requirement between the $\not{E}_T$ and the closest jet (see Table IX) is designed to reduce this background. There is no intrinsic $\not{E}_T$ in these events, however jet energy can be lost in cracks, and the measurement of the jet energy can fluctuate, faking a $\not{E}_T$ signal. In these cases, the $\not{E}_T$ tends to point towards one of the two jets in the event. In order to reduce this background, the $\not{E}_T$ requirement in CDF is raised to 50 GeV when the azimuthal angle between the $\not{E}_T$ direction and a jet is less than 20°, see Fig. 67.

D0's approach is different. First of all, the H_T requirement is more effective than a minimum number of jets requirement because the jets in Drell-Yan + jets events are in general softer than the jets in $t\bar{t}$ events, for sufficiently high top mass. Furthermore, to reduce the Drell-Yan background, the $\not{E}_T$ requirement is raised to 25 GeV for dielectron events. Recall that in the $\mu\mu$ channel, no cut is made on $\not{E}_T$ because the muon energy measurement is poor.

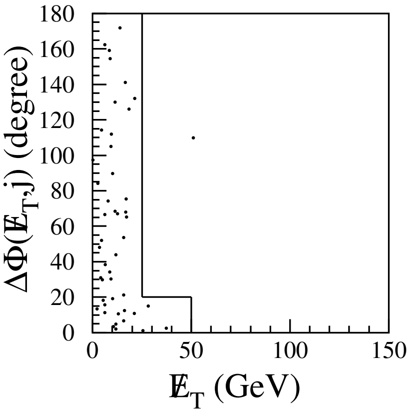

FIG. 67. Distribution of the azimuthal angle between the $\not{E}_T$ and the closest jet as a function $\not{E}_T$ for $Z \to ll$ events with two jets. The $\not{E}_T$ characteristics of these events should closely resemble those of Drell-Yan events. This is CDF data with an integrated luminosity of 19 pb^{-1}. Also shown is the boundary of the CDF $\not{E}_T$ requirement. From the CDF collaboration, F. Abe *et al.*, 1994a.

4. WW background

The expected background from diboson production, WW, WZ, and ZZ, is small but not at all negligible. The WW process is the dominant diboson background to the $t\bar{t}$ dilepton signature. The WZ and ZZ production cross-sections are expected to be lower and are further suppressed by the small $Z \to ll$ branching ratio, see the discussion in Section V.D. Neither collaboration has published evidence for the process $p\overline{p} \to W^+W^-$, however the cross-section expected from theory is slightly higher, of order 10 pb, than the equivalent $t\bar{t}$ cross-section, which is expected to be $\sigma(t\bar{t}) \approx 5$ pb for $\mathrm{M}_{top} = 175$ GeV/c^2, (see Fig. 21).

WW events include large transverse momentum leptons and $\not{E}_{\mathrm{T}}$. In Fig. 68 we show the expected distributions of $\not{E}_{\mathrm{T}}$ and $\Delta\phi$ for $t\bar{t}$ and WW events. The kinematic properties of the two processes are very similar. The most effective way to reduce these backgrounds is to require the presence of high transverse momentum jets. The H_T requirement imposed by D0 is more effective in discriminating against WW than the simple minimum-number-of-jets requirement employed by CDF. The remaining background is estimated entirely from Monte Carlo, using the theoretical expectations for the WW cross-section.

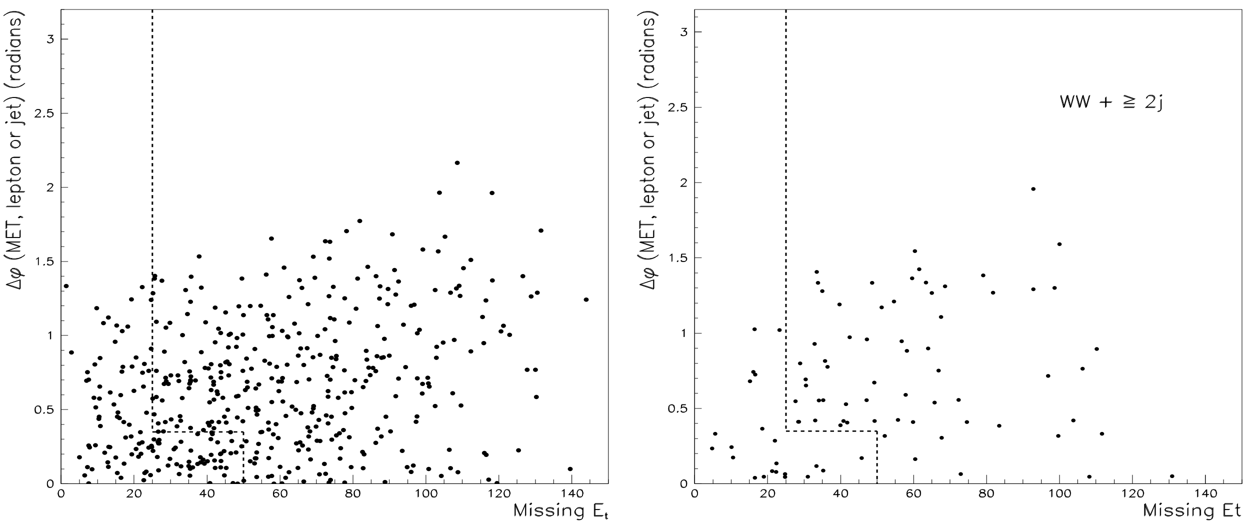

FIG. 68. CDF Monte Carlo expectations for $\Delta\phi$ versus $\not{E}_{\mathrm{T}}$ for (a) $t\bar{t}$ with $\mathrm{M}_{top} = 180$ Gev/c^2, and (b) WW + $\geq$ + 2 jet production. The vertical axis is the smallest of the azimuthal angles between the $\not{E}_{\mathrm{T}}$ vector and the leptons or jets. The symbol MET in the vertical-axis label refers to the $\not{E}_{\mathrm{T}}$.

5. $b\bar{b}$ and fake lepton backgrounds

Doubly semileptonic decays in $b\bar{b}$ events and events with fake leptons constitute another important background to the dilepton signature. These backgrounds are considerably reduced by requiring two isolated high transverse momentum leptons, and high $\not{E}_{\mathrm{T}}$. The $b\bar{b}$ background is calculated from Monte Carlo, normalized to the rate of lower momentum $b\bar{b} \to$ dileptons events. The probability of finding two high momentum isolated fake leptons in an event is exceedingly small. The main fake dilepton background is due to $W+$ jets events, where one of the leptons is from the $W \to l\nu$ decay, and one of the jets is misidentified as a lepton. The background is then estimated by multiplying the number of observed $W+$ jets events by the probability for a jet to fake the isolated electron or muon signature as determined from samples of jet events. This probability is typically of order 10^{-4}.

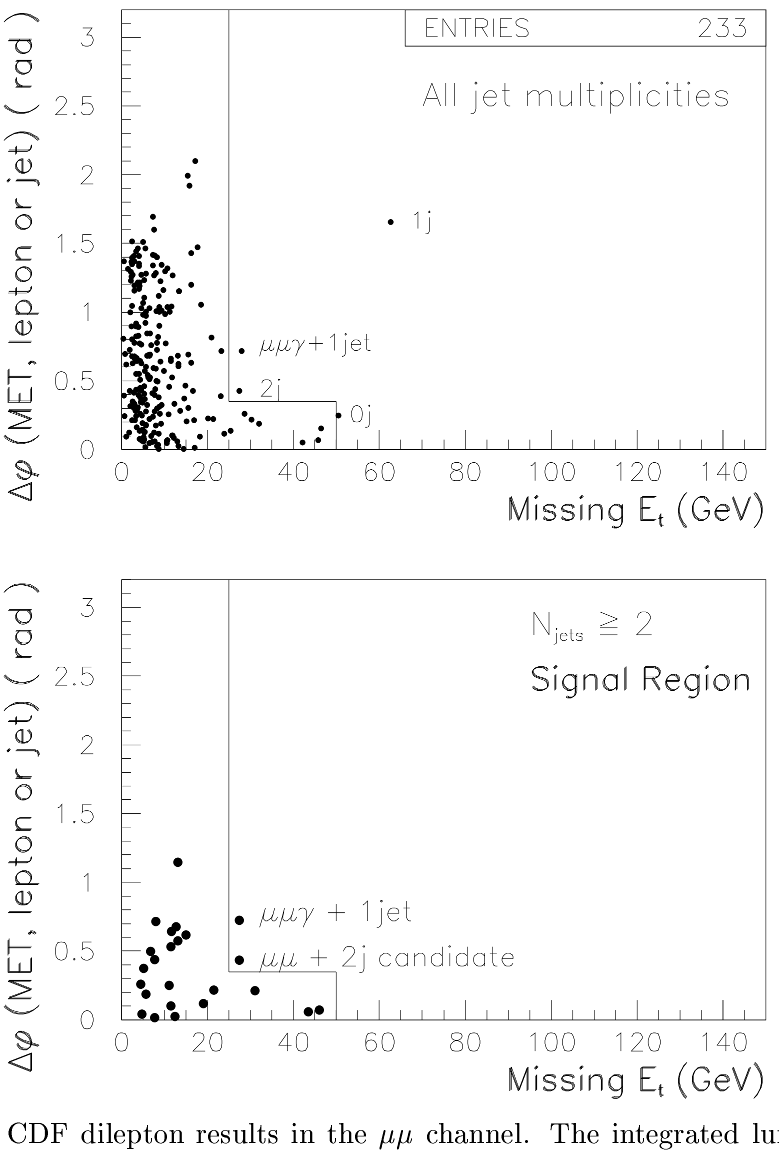

FIG. 69. CDF dilepton results in the $\mu\mu$ channel. The integrated luminosity is 67 pb^{-1}. From Roser, 1995. The vertical axis is the smallest of the azimuthal angles between the $\not\!\!E_T$ vector and the leptons or jets. The symbol MET in the vertical-axis label refers to the $\not\!\!E_T$.

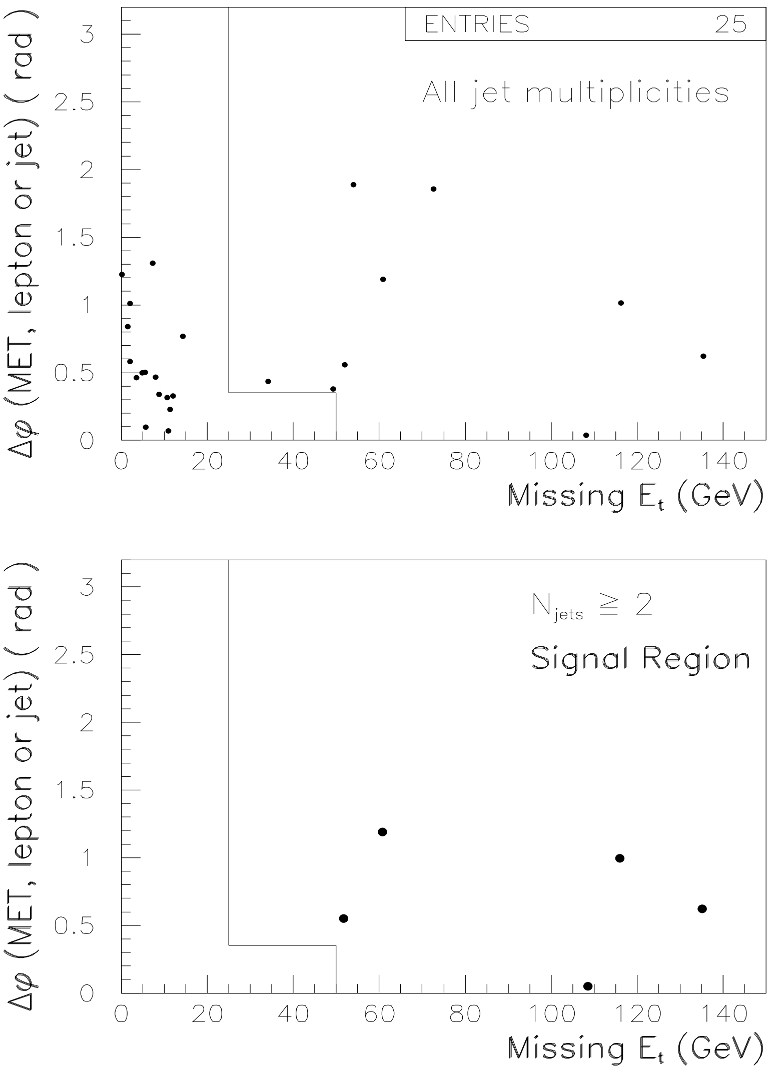

FIG. 70. CDF dilepton results in the $e\mu$ channel. The integrated luminosity is 67 pb^{-1}. From Roser, 1995. The vertical axis is the smallest of the azimuthal angles between the $\not{E}_T$ vector and the leptons or jets. The symbol MET in the vertical-axis label refers to the $\not{E}_T$.

	CDF	D0
Background Source		
$Z \to \tau\tau$	0.38 $\pm$ 0.07	0.24 $\pm$ 0.07
WW	0.21 $\pm$ 0.07	0.06 $\pm$ 0.03
Fakes, $b\bar{b}$	0.26 $\pm$ 0.16	0.12 $\pm$ 0.04
$Z \to ee$ or $\mu\mu$	-	0.24 $\pm$ 0.03
Drell Yan	0.44 $\pm$ 0.28	-
Total background	1.3 $\pm$ 0.3	0.65 $\pm$ 0.15
$t\bar{t}$ expectation, M_{top} = 180 GeV/c^2	2.4	1.2
Data	5 $e\mu$ 1$\mu\mu$	2 $e\mu$ 1 $\mu\mu$

TABLE X. Background sources, $t\bar{t}$ expectations, and event yields in the CDF (Roser, 1995) and D0 (Narain, 1995) dilepton analyses. One additional CDF candidate event, consistent with the $Z \to \mu\mu\gamma$ hypothesis, is not included in this table, see the discussion in the text. The integrated luminosity for the CDF data is 67 pb^{-1}. For the D0 data, the integrated luminosity is 55.7 pb^{-1} for ee, 44.2 pb^{-1} for $\mu\mu$, and 47.9 pb^{-1} for $e\mu$. The $t\bar{t}$ expectations are obtained using the calculation of $\sigma(t\bar{t})$ from Laenen, Smith, and van Neerven, 1994.

6. Results

The acceptance for the CDF analysis for M_{top} = 180 GeV is $\epsilon = (0.87 \pm 0.10)\%$, where this acceptance includes the branching ratio for the dilepton mode (4/81, see Table III). The equivalent acceptance for D0 is $(0.55 \pm 0.04)\%$. With these acceptances, and given the integrated luminosities and the theoretical expectations for $\sigma(t\bar{t})$, both experiments are sensitive to $t\bar{t}$ production for top masses up to $M_{top} \approx 200$ GeV/c^2. The results of the CDF and D0 $t\bar{t}$ searches in the dilepton channel are summarized in Table X.

CDF finds 7 dilepton candidates in 67 pb^{-1} with 1.3 ± 0.3 expected background events. Of these 7 candidate events, five are $e\mu+$ jets events and two are $\mu\mu+$ jets events. One of the two $\mu\mu$ events looks very much like a radiative Z decay, $Z \to \mu\mu\gamma$, since the invariant mass of the $\mu\mu\gamma$ is 86 ± 7 GeV/c^2. Although the background from radiative Z decays was estimated to be less than .04 events, CDF conservatively a-posteriori removes this event from the top candidate sample and is left with 6 events (5 $e\mu$ and one $\mu\mu$). Acceptances for top are such that 60% of $t\bar{t}$ are expected in $e\mu$ and 40% in $ee/\mu\mu$. Figs. 69 and 70 show the CDF data in the $\Delta\phi - \not{E}_T$ plane. As can be seen from these figures, the $e\mu$ channel is much cleaner due to the absence of the Drell-Yan contribution.

D0 finds 3 candidates in approximately 50 pb^{-1} with $.65 \pm 0.15$ expected background events. Of these three events, two are $e\mu+$ jets and one is $\mu\mu+$jets. This is consistent with the ratio of expected number of events, $e\mu : ee : \mu\mu = .34 : .25 : .11$ for a 200 GeV top quark.

Thus, both experiments see an excess of dilepton events over the total background prediction. The size of this excess is loosely consistent with expectations for $t\bar{t}$. It is interesting to notice that there are some significant differences in the CDF and D0 background sources,

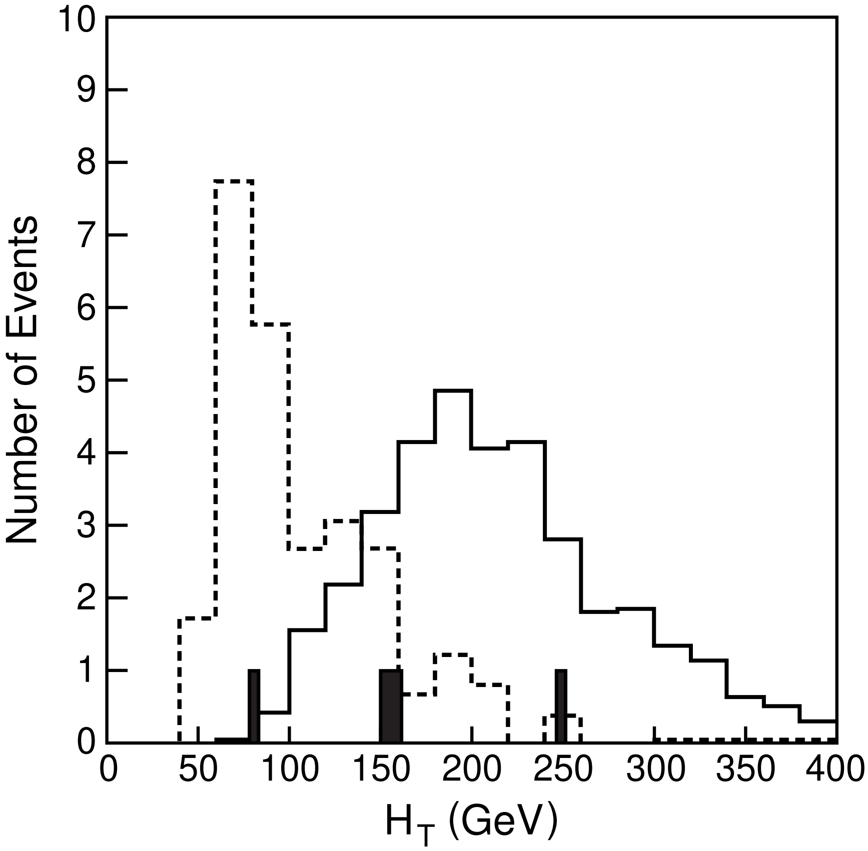

FIG. 71. Distributions of H_T for dilepton data for D0 (Grannis, 1995) The integrated luminosity is ≈ 50 pb^{-1}. The solid line is the expected H_T distribution for top events in the dilepton channel. The dashed line is the expected backgrounds and the solid histogram is the data. See text for details.

see Table X. The highest background source in the CDF analysis is due to Drell-Yan events. This background is negligible in D0, probably due to the D0 H_T requirements, the stricter $\not{E}_T$ requirement in the ee channel, and the hermeticity of the D0 detector. Also, $Z \rightarrow ee$ and $\mu\mu$ are totally eliminated by the CDF invariant mass requirement, while they make up a substantial fraction of the total background in D0.

As partial evidence that the excess of events is not due to a background fluctuation or to underestimation of the backgrounds, we present in Fig. 71 the H_T distribution of dilepton events from D0. As was discussed earlier, in D0 H_T is defined as the scalar sum of the transverse energy of all of the jets in the event + the E_T of the highest E_T electron (for the ee and $e\mu$ channels). As we argued throughout this Section, and as shown in Fig. 62, H_T is a powerful discriminant between signal and background. The D0 candidate events are distributed in H_T in a manner more consistent with $t\bar{t}$ than background.

In addition, in the six CDF dilepton candidate events, there are five jets (in three events) that are tagged as b-jets by the algorithms which will be described in Section VIII.B. This is to be compared with the expectation of approximately 0.5 b-tagged jets if all six events were background, and approximately 3.6 b-tagged jets if all six events were $t\bar{t}$. This suggests that the excess of dilepton + jets events over the background prediction is correlated with the presence of b-quarks in the event, as expected if the excess were due to $t\bar{t}$.

B. Lepton + jets + b-tag

As was discussed in Section V.E.4, one of the most effective ways of isolating a top signal in the lepton + jets mode ($t\bar{t} \to q\bar{q}\ l\nu\ b\bar{b}$) is to tag the b-quarks in $t\bar{t}$ events. This can be achieved by searching for leptons from the semileptonic decay of b-quarks (lepton tagging), or by exploiting the long lifetime of b-hadrons (vertex tagging). Lepton tagging has been used by both CDF and D0 to extract a top signal; vertex tagging, which requires momentum analysis, as well as precise vertex detection capabilities, has been performed by CDF only. In Section VIII.B.1 we will review the CDF and D0 selections of lepton + jets data, before the b-tag requirement. The results of the b-tag analyses on these data are then discussed in Sections VIII.B.2 and VIII.B.3 for lepton and vertex tagging respectively. A brief summary of the tagging searches, as well as results of cross-checks performed on samples of Z+ jets, are presented in Section VIII.B.4.

1. Selection of lepton + jets data before b-tagging

The CDF and D0 selections of the isolated e or μ + jets data for the b-tagging analyses are summarized in Table XI. The event selection employed by the two collaborations are similar. In principle, one would expect to detect four jets in a $t\bar{t} \to$ lepton + jets event; however, as discussed in Section V.B.2, the detected number of jets can be smaller (see for example Fig. 35). This is because jets from top decay sometime have E_T below threshold, or two or more of these jets can be close enough to each other that they are reconstructed as a single jet. Therefore, in order to maintain high efficiency, the minimum number of jets required by both CDF and D0 is three rather than four. The one significant difference in the selection requirements between the two experiments is that D0 imposes a further requirement on the minimum scalar sum of the transverse energy of all jets in the event (H_T, see Table XI). This requirement is expected to improve the rejection against the dominant W + jets background, especially for high top quark masses (see Fig. 46). No such requirement is imposed on the CDF data in order to maintain high $t\bar{t}$ detection efficiency for M_{top} as low as 100 GeV/c^2, and because of the superior background rejection capabilities of the CDF vertex tagging analysis.

The selections summarized in Table XI yield data samples consisting mostly of W+ jets events, as well as a contamination from QCD events, and hopefully also a $t\bar{t}$ component. The QCD contamination is due to events with fake leptons, as well as semileptonic decays of b-quarks in $p\bar{p} \to b\bar{b}$ events. In almost all of the channels, these events are estimated to contribute approximately 10% to the event sample; the exception is the D0 μ+ jets channel, where this background is a factor of 2-2.5 larger, due to the poor resolution of the D0 muon momentum measurement. These data samples also include small contributions from Z and diboson events.

The numbers of expected $t\bar{t}$ events in the data samples (see Table XI) depend on M_{top}, since both the $t\bar{t}$ production cross-section and acceptance depend on M_{top}. Given the theoretical expectations for the $t\bar{t}$ production cross-section, the expected signal-to-background in these data samples before applying b-tagging (*pre-tag* samples) varies between approximately 1/16 and 1/3, depending on top mass, and selection details.

	CDF	D0
Lepton E_T or P_T	≥ 20 GeV	≥ 20 Gev (e); ≥ 15 GeV (μ)
Lepton rapidity coverage	$\lvert\eta\rvert \leq 1^{(a)}$	$\lvert\eta\rvert \leq 2$ (e); $\lvert\eta\rvert \leq 1.7$ (μ)$^{(b)}$
$\not\!\!E_T$	≥ 20 GeV	≥ 20 GeV
Number of jets	≥ 3	≥ 3
Jet E_T	≥ 15 GeV (uncorrected)	≥ 20 GeV (corrected)
Jet rapidity coverage	$\lvert\eta\rvert \leq 2$	$\lvert\eta\rvert \leq 2$
Jet cone clustering radius	0.4	0.5
H_T	-	≥ 140 GeV
Integrated luminosity	67 pb^{-1}	48 pb^{-1} (e); 44 pb^{-1} (μ)
No. of events in data sample	203	66
No. of expected $t\bar{t}$ events, M_{top} = 140 GeV/c^2	≈ 95	≈ 22
No. of expected $t\bar{t}$ events, M_{top} = 200 GeV/c^2	≈ 13	≈ 6

TABLE XI. CDF and D0 lepton + jets requirements for the b-tag analysis. The variable H_T in D0 is defined as the scalar sum of the E_T of all the jets. The expected number of top events are derived from the theoretical estimate of the $t\bar{t}$ cross-section (Laenen, Smith, and van Neerven, 1994) and the calculated acceptances. Notes : $^{(a)}$ the CDF muon chambers only cover $\approx 2/3$ of the solid angle for $0.6 < |\eta| < 1$; $^{(b)}$ Muons in D0 are restricted to $|\eta| < 1$ for the last $\approx 70\%$ of data, due to ageing of the forward muon chambers.

The dominant physics background in the lepton + jet + b-tag channel is due to the associated production of a W boson and a pair of heavy quarks ($WQ\bar{Q}$, $Q = b$ or c, see Section V.E.4, Fig. 52). As discussed in Section V.E.4, the fraction of $W+\geq 3$ jets events containing a $Q\bar{Q}$ pair is expected to be of order 3% for $Wb\bar{b}$ and 5% for $Wc\bar{c}$. Therefore, given the signal-to-background levels in the lepton + ≥ 3 jets samples before demanding a b-tag, a $t\bar{t}$ signal is expected to stand out after application of a b-tag requirement, provided that instrumental backgrounds can be kept under control.

2. Lepton tagging in CDF and D0

Leptons from b-quarks in $t\bar{t}$ arise from direct ($b \rightarrow cl\nu$) or cascade ($b \rightarrow c \rightarrow sl\nu$) decays. Given the b- and c-quark semileptonic branching ratios, and including the contribution from semileptonic decays of c-quarks from $W \rightarrow c\bar{s}$, there is on average approximately one lepton (e or μ) from b or c decay in each $t\bar{t} \rightarrow$ lepton + jets event in addition to the lepton from W decay. These additional leptons tend to have low transverse momentum, see Fig. 49, and to be non-isolated because of the presence of nearby hadrons from the b-quark fragmentation and the b-hadron decay, (see Fig. 72). Detection of these leptons is therefore more difficult than detection of the isolated high P_T leptons from W decays.

There are two main differences in the lepton-tagging algorithms developed by the two collaborations. The first difference is that the D0 analysis only tags muons, whereas CDF tags both muons and electrons. This is because detection of non-isolated electrons in D0 is not as effective as in CDF, mostly due to the absence of a magnet for momentum measure-

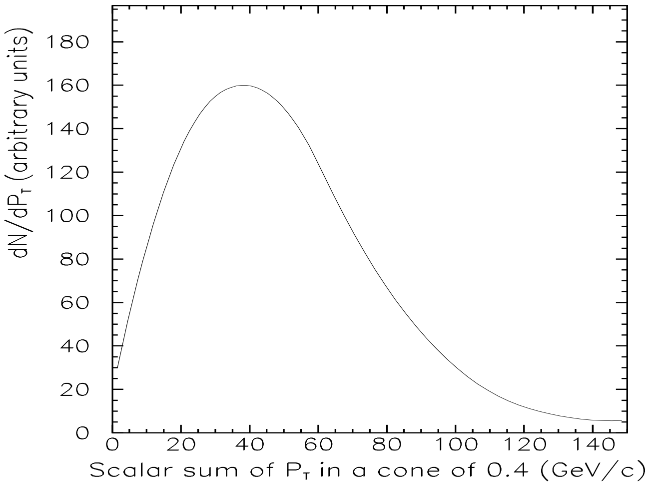

FIG. 72. The expected scalar sum of the transverse momenta of all particles in the $t\bar{t}$ final state within a cone of radius 0.4 of the lepton from $b \to cl\nu$ or $b \to c \to sl\nu$. From the ISAJET Monte Carlo, for M$_{top}$ = 175 GeV/c^2. The momenta of the lepton and the neutrino are not included in the sum.

ment. In CDF electrons from b-decays can be identified with sufficient background rejection. However, the efficiency for detecting these electrons is lower than the efficiency for detecting muons, and only of order 30% of the lepton tagging efficiency in CDF is due to electron tags. The second difference between the two experiments resides in the minimum P$_T$ requirement for these tagging leptons. In D0, this requirement is set at 4 GeV/c, which corresponds to the minimum P$_T$ for a muon to penetrate the D0 muon detectors; in CDF this minimum P$_T$ requirement is set at 2 GeV/c. The lower P$_T$ requirement improves the efficiency for detecting muons from cascade decays, especially for low top quark masses, (see Fig. 49), however it also results in higher background levels.

Additional requirements are imposed in the D0 analysis to reject events with tagging muons collinear or back-to-back with the direction of the $\not{E}_T$ vector. These requirements are designed to reject QCD events. The rapidity coverages for tagging leptons in the two experiments are the same as those for the high P$_T$ leptons from W decays, see Table XI. For M$_{top}$ > 140 GeV/c^2, the $t\bar{t}$ lepton-tagging efficiency is 20% for both experiments. The greater muon coverage of the D0 detector makes up for the higher P$_T$ threshold and the absence of electron-tags.

Backgrounds to b-tagging were discussed extensively in Section V.E.4. The $WQ\bar{Q}$ backgrounds in both CDF and D0 are calculated by assuming that the heavy flavor content of jets in W + jets events is the same as that of generic jets. This corresponds to the Method I background estimate of Section V.E.4, and is expected to yield an over-estimate of the background. In D0, a tagging rate per jet as a function of jet E$_T$ is defined as the ratio of the number of tagged jets divided by the total number of jets as a function of E$_T$, (see Fig. 73). The background to the lepton tagged signal is then calculated by convoluting this tagging rate with the E$_T$ spectrum of jets in the $W+ \geq 3$ jets sample. As discussed in Section V.E.4, this procedure yields simultaneously an estimate of the instrumental and $WQ\bar{Q}$ backgrounds.

A similar procedure is used in CDF, with the difference that track-tag rates instead of jet-tag rates are used. The track-tag rate is defined as the ratio of the number of tracks in jet events that are tagged as leptons divided by the total number of tracks. To calculate the background, electron and muon track-tag rates as a function of P_T are convoluted with the P_T spectrum of tracks in the $W+ \geq 3$ jets sample. The CDF muon track-tag rate is displayed in Fig. 74; the analogous electron track-tag rate is considerably smaller, see F. Abe *et al.*, 1994a.

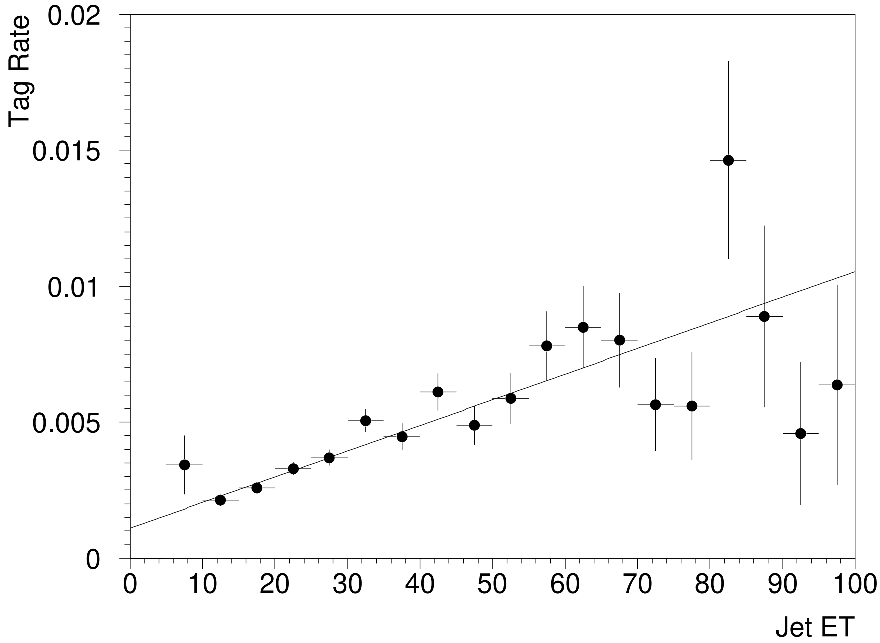

FIG. 73. Tagging rate for jets as a function of E_T in the D0 detector as measured from a sample of fake electron + jets events. From Snyder, 1995a.

An additional physical background to the tagged $W+$ jets search is due to production of a W and a single c-quark, $W+$ charm, (see Fig. 51). In the D0 analysis it is assumed that this background is automatically included when the jet-tag rate is convoluted with the jet E_T spectrum. On the other hand, this background is calculated explicitly by CDF and is added in separately.

A background contribution from $Z \rightarrow \mu\mu$ events is also present in D0. The two muons can result in misinterpreting such an event as $W \rightarrow \mu\nu$ event with a μ tag. The poor muon momentum resolution does not allow for a clean removal of these events via an invariant mass cut, as is done in CDF. Just as in the D0 dilepton analysis (see Section VIII.A), these events are identified using a global event χ^2-test for consistency with the Z hypothesis. Since the Z removal procedure is not 100% efficient, the D0 background estimate in the lepton + jets + b-tag search also includes a contribution from residual $Z \rightarrow \mu\mu$ events in the sample. Additional small backgrounds are due to all sources of dileptons discussed in Section VIII.A (e.g. $Z \rightarrow \tau\tau$, dibosons, $b\bar{b}$). These backgrounds are expected to be small. They are included in the CDF background estimate, and taken as negligible by D0.

Both CDF and D0 see an excess of tags in the $W+ \geq 3$ jets samples over their respective background estimates. The D0 collaboration finds 6 events on an expected background of

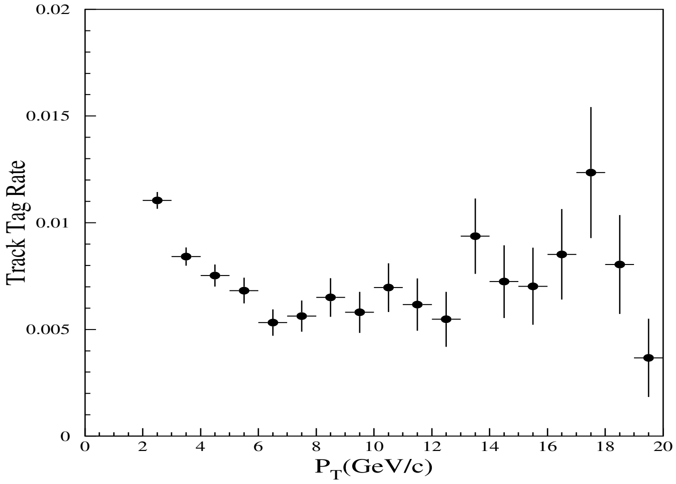

FIG. 74. Muon track tagging rate as a function of P_T in the CDF detector as measured from a sample of jet events. From F. Abe *et al.*, 1994a.

1.2 ± 0.2; the CDF collaboration finds 23 tags in 22 events, with an expected background of 15.4 ± 2.0 tags. The most powerful check of the background calculation procedure is to repeat the exercise for W events with only one or two jets, where the $t\bar{t}$ content of the data sample is expected to be very small. This is summarized in Fig. 75 for D0 and Fig. 76 for CDF. The background calculations reproduce the expected tagging rates in W events with low jet multiplicity.

In this Section and in Section V.E.4, we have argued that the $WQ\bar{Q}$ background is overestimated in both the CDF and D0 analyses, yet the background predictions in the $W+$ 1 and $W+$ 2 jets samples are in good agreement with the data. The reason for this is that the dominant background in these analyses is due to fake leptons, not $WQ\bar{Q}$. For example, if the CDF backgrounds were to be calculated using the best theoretical input for $WQ\bar{Q}$, the background estimate would have been reduced by only about 10%, independently of jet multiplicity (F. Abe *et al.*, 1994a). This is well within the 20% systematic uncertainty assigned to the background calculation.

The sizes of the excesses of events seen by the two collaborations are loosely consistent with expectations for $t\bar{t}$. The D0 collaboration sees an excess of 4.8 events; the number of expected tagged $t\bar{t}$ events varies between 4.4 and 1.2 for M_{top} between 140 and 200 GeV/c^2. The CDF excess is 7.6 tags, to be compared with a $t\bar{t}$ expectations of between 19 tags (M_{top} = 140 GeV/c^2) and 2.6 tags (M_{top} = 200 GeV/c^2).

Despite the fact that the lepton tagging efficiencies are comparable in the two experiments, the signal-to-background is better for the D0 analysis. This is mostly because backgrounds to the detection of low P_T muons are lower in D0 than in CDF. This fact is best illustrated by comparing Fig. 73 with Fig. 74. The muon tagging rate in D0 is a fraction of 1% per jet; in CDF it is a fraction of 1% per track. There are three main reasons for the lower muon background in D0 : (i) muons in D0 have to traverse more steel than in CDF, so that background from hadronic punch-through is lower in D0 than CDF; (ii) the D0 detector is more compact, resulting in a lower probability for decays in flight of pions

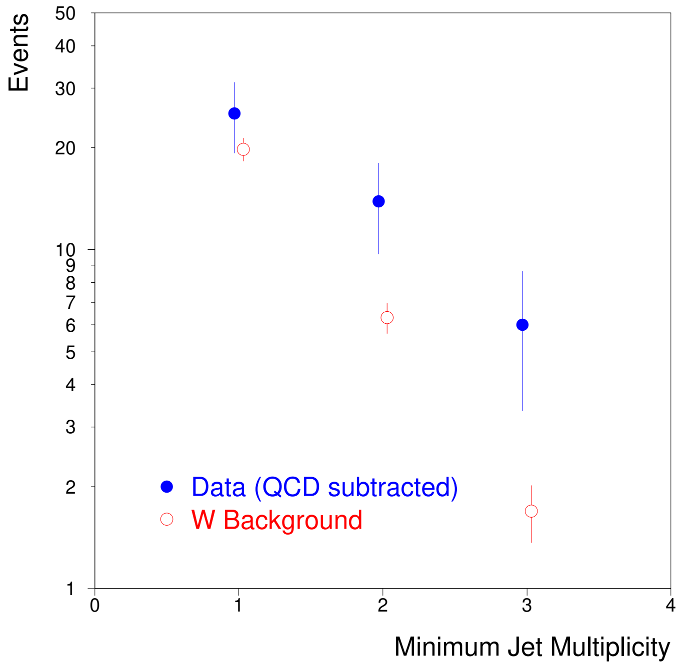

FIG. 75. Comparison between the observed number of muon tags and the background expectation in $W+$ jets event as a function of jet multiplicity for D0 data. The H_T requirement (see Table XI) has been removed for these data. Note that the horizontal axis is in terms of *minimum jet multiplicity*, e.g. the 2-jet bin includes all events with 2 or more jets. From Snyder, 1995a.

and kaons; (iii) the momentum of the muon is measured after the decay-in-flight in D0, whereas in CDF, some average of the momentum of the parent pion and daughter muon is often measured in the drift chamber. The background rate per event, dominated by decays in flight and punch-through, is 1.8% in D0 and 7.6% in CDF.

In addition to these instrumental effects, the different choice of requirements between CDF and D0 contribute to differences in signal-to-background. The D0 pre-tag event sample with the H_T requirement is expected to contain a higher fraction of $t\bar{t}$ events, for sufficiently high top mass. On the other hand, there is no requirement on H_T in CDF, in order to maintain good efficiency for low top masses (M_{top} < 120 GeV/c^2). For example, for M_{top} = 200 GeV/c^2, the $t\bar{t}$ contents of the D0 and CDF pre-tag samples are expected to be approximately 9% and 6% respectively, see Table XI.

Furthermore, the minimum P_T requirement for lepton tags is lower in the CDF analysis than in the D0 analysis (2 GeV/c vs. 4 GeV/c). Again, the CDF requirement was chosen to maintain efficiency for low top mass, where leptons from cascade decays have very low transverse momenta, (see Fig. 49). If the CDF requirement were to be raised to 4 GeV/c, the background would be reduced by a factor of $\approx$ 1.8, while the tagging efficiency for M_{top} > 130 GeV/c^2 would be lowered by approximately 20% only (F. Abe *et al.*, 1994a). An excess of events in the CDF lepton tag analysis is also present when the minimum P_T

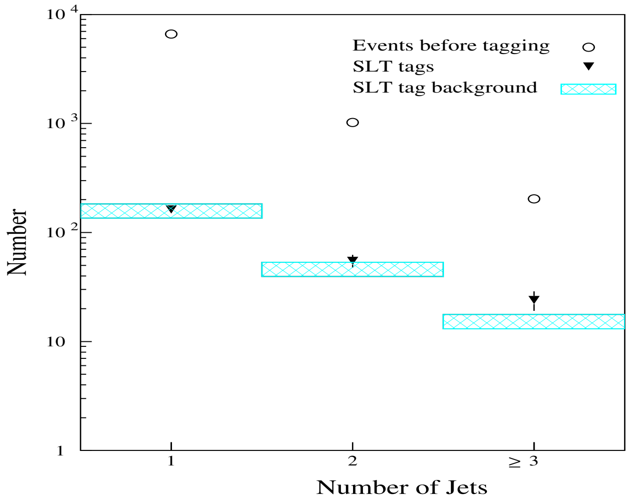

FIG. 76. Comparison between the observed number of lepton tags and the background expectation in $W+$ jets event as a function of jet multiplicity for CDF data (Kestenbaum, 1996).

requirement is raised to 4 GeV/c. In this case, 15 tags in 14 events are observed, with a background of 8.7 ± 1.8 tags (Kestenbaum, 1996).

3. Displaced-vertex tagging in CDF

The most powerful method employed by the CDF collaboration to extract a top signal in the lepton + jet channel is to search for secondary vertices from b-quark decay (vertex tagging). This is made possible with the precise tracking information obtained from a silicon vertex detector.

CDF is the first, and so far the only, experiment to operate such a detector in a hadron collider. The first silicon vertex detector (SVX) at CDF was installed in 1992 prior to the beginning of Run Ia. The SVX (Amidei *et al.*, 1994) is a four-layer cylindrical detector which is 51 cm long. The four layers are at distances of 3.0, 4.2, 5.7, and 7.9 cm from the beamline. Axial microstrips with 60 μm pitch on the three innermost layers and 55 μm pitch on the outermost layer provide precision track reconstruction in the plane transverse to the beam. The single hit resolution is 13 μm, and the impact parameter resolution, for high momentum tracks is 17 μm. The SVX detector suffered significant radiation damage, and was replaced in 1993, during the accelerator shutdown period between Runs Ia and Ib, by a very similar detector (SVX$'$, Azzi, 1994) equipped with radiation-hard electronics.

The vertex tagging algorithm used by CDF is based on reconstruction of displaced vertices using information from both the central tracking chamber and the SVX (or SVX$'$). At the Tevatron, $p\bar{p}$ interactions are spread along the beamline with standard deviation $\sigma \approx 30$ cm, so that the geometrical acceptance of the vertex detector is about 60% for $p\bar{p}$ interactions. This geometrical effect turns out to be the largest source of efficiency loss in tagging $t\bar{t}$ events.

The position of the primary vertex is needed before searching for a possible secondary vertex. The transverse spreads of the colliding p and $\bar{p}$ beams result in a luminous region in the transverse plane which is Gaussian in shape with $\sigma \approx 36$ μm. The position and size of this region varies somewhat from store to store, and is monitored with an accuracy of order 10 μm. On an event-by-event basis, knowledge about the position of the primary vertex is improved by performing a fit using information from tracks consistent with originating from the primary vertex. The accuracy of the event-by-event determination of the position of the primary vertex in the transverse plane depends on the number of tracks available to the fit, and varies between 6 and 36 μm.

The vertex tagging algorithm operates on combinations of at least two tracks with impact parameter at least three standard deviations different from zero. Constrained vertex fits are performed on these track combinations in an attempt to find one or more sets of tracks which are consistent with originating from a secondary vertex. Selection criteria are applied to reject tracks from decays of Λ and K^0_s. Results of the vertex fit include the distance in the transverse plane of the secondary vertex from the primary vertex (L_{xy}) and its uncertainty (σ_{lxy}). For a good secondary vertex which results in a b-tag, $\mathrm{L}_{xy}/\sigma_{lxy}$ is required to be > 3. The typical accuracy on the determination of the position of a secondary vertex is $\sigma_{lxy} \approx 130$ μm. This is much smaller than the distance travelled by a b-hadron in a top event (typically a few mm, see Fig. 50), thereby allowing for efficient identification of secondary vertices from b-hadron decay. There are two possible kind of vertex tags, *positive tags* and *negative tags*, (see Fig. 77). Only positive tags are consistent with originating from the decay of a long-lived particle produced at the primary vertex. Negative tags, however, provide useful information on the performance of the b-tagging algorithm, as we will discuss below.

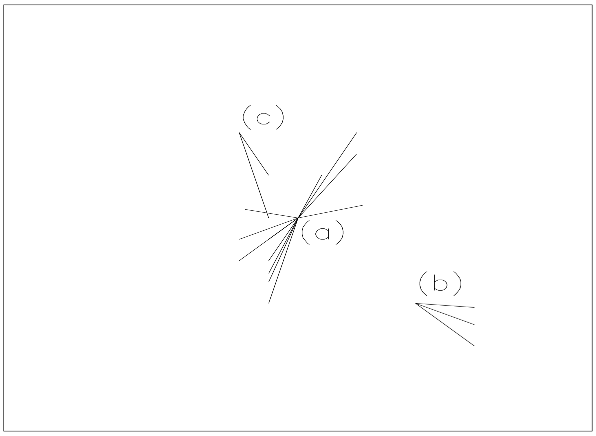

FIG. 77. An idealized sketch of vertex tagging in the transverse plane. The tracks from the primary vertex (a) are used to improve on the accuracy of the determination of the position of the primary vertex. Vertex (b) is a secondary vertex which is consistent with the hypothesis that it originates from the decay of a long-lived particle produced at the primary. This is a *positive tag*. On the other hand, vertex (c), although detached from the primary, is not consistent with the decay of a long-lived particle from the primary. Vertex (c) is an example of a *negative tag*, which is due to track mismeasurements. In a $t\bar{t} \to$ lepton + jets event, the tracks from vertex (a) in general originate from the underlying event or from the hadronization of the q or $\bar{q}$ from the decay of the W in $t \to Wb, W \to q\bar{q}$.

The capabilities of the CDF silicon vertex detector for detection of secondary b-vertices are best illustrated in Fig. 78, which summarizes the CDF measurement of the lifetime of b-hadrons from the decay $B \to J/\Psi + X; J/\Psi \to \mu\mu$. The proper decay length (λ) of the b-hadron is reconstructed from the position of the $\mu\mu$ vertex as

$$\lambda = L_{xy} \quad \frac{M_{J/\Psi}}{P_T^{J/\Psi} F(P_T^{J/\Psi})}$$

where $M_{J/\Psi}$ is the J/Ψ mass, $P_T^{J/\Psi}$ is the J/Ψ transverse momentum, and F is a Monte-Carlo determined correction factor which accounts for the undetected particles in the $B \to J/\Psi + X$ decay. The result of the lifetime fit, $\tau_B = 1.46 \pm 0.06 \pm 0.06$ ps, is one of the world's most precise measurements of this quantity, and is consistent with the results from LEP.

The CDF vertex tag efficiency in top events is $\epsilon_{tag} = (42 \pm 5)\%$. This efficiency is defined as the probability of finding at least one (positive) displaced vertex within one of the jets in a $t\bar{t}$ event with ≥ 3 jets. The vertex tag efficiency is a factor of two larger than the analogous efficiency of the CDF and D0 lepton tag algorithms discussed in the previous Section.

The value of ϵ_{tag} is determined from a Monte Carlo simulation of the response of the detector to $t\bar{t}$ events. In order to verify the reliability of the detector simulation, a number of studies of b-tagging are performed in samples of $b \to l$ events. The results of these studies are compared with expectations from a Monte Carlo simulation of this process, and the

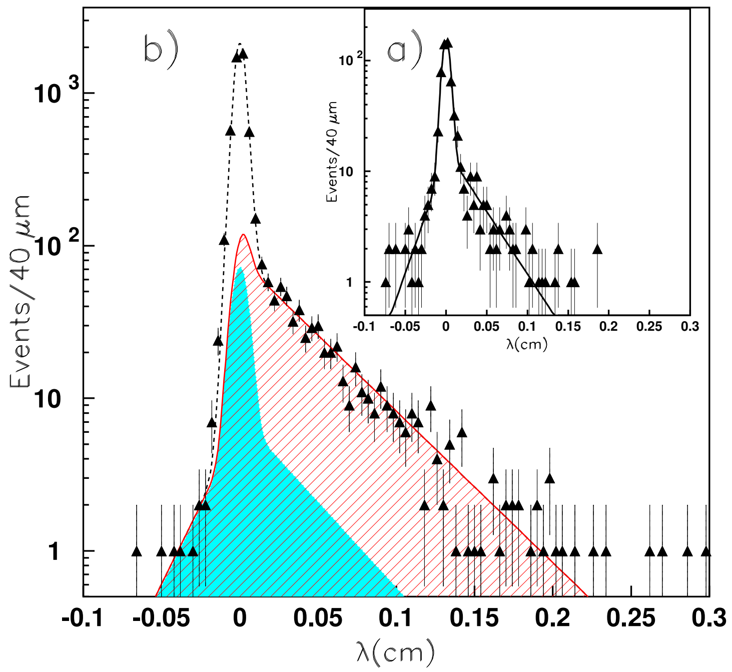

FIG. 78. CDF measurement of the b-hadron lifetime from $B \to J/\Psi + X$ decays. (a) The distribution in λ, the proper decay length, of data in the J/Ψ sideband regions. The solid line shows the result of the fit. (b) The distribution in λ, of data in the J/Ψ region. The curves are the result of the fit. The lightly shaded area is for $B \to J/\Psi + X$ events. The darkly shaded area is for the non-J/Ψ background. The large J/Ψ component at $\lambda \approx 0$ is due to prompt J/Ψ production and to $\chi \to J/\Psi$ decays. From F. Abe *et al.*, 1993d.

level of agreement found between the data and Monte Carlo is used to set the systematic uncertainty on ϵ_{tag}. The largest source of inefficiency is due to the long luminous region of the Tevatron ($\sigma = 30$ cm). Since the vertex detector is only 51 cm long, approximately 40% of the interactions occur outside its geometrical coverage.

Note that the tagging efficiency reported in the first CDF publications on vertex tagging in top events (F. Abe *et al.*, 1994a) was considerably smaller, $\epsilon_{tag} = (22 \pm 6)\%$. This value of the tagging efficiency was underestimated by 15%, due to a mistake in the Monte Carlo simulation. In addition, the tagging algorithm used in the earlier analysis has been substantially improved, and the performance of the SVX$'$ in terms of efficiency and signal-to-background is somewhat better than that of SVX.

In the lepton tag analyses described in the previous Section, the instrumental and $WQ\bar{Q}$ backgrounds were estimated simultaneously under the assumption that the heavy flavor content of generic jets is the same as the heavy flavor content of jets in W events (Method I, see Section V.E.4). As has been argued before, this method overestimated the size of the $WQ\bar{Q}$ background. On the other hand, the Method II background calculation, which was also discussed at length in Section V.E.4, relies on a theoretical estimation of $WQ\bar{Q}$. To the extent that the instrumental background in the lepton tag analysis is larger than the $WQ\bar{Q}$ background, numerically the Method I and Method II backgrounds are not very different. For the vertex tag analysis, however, this is not the case. Therefore, the CDF collaboration has chosen to calculate the background in this channel using Method II.

The instrumental background, i.e. the background due to false tags in light quarks or gluon jets, is estimated from the negative tagging rate as measured in a sample of generic jets. Since negative tags are almost exclusively due to tracking mismeasurements, and since these mismeasurements are equally likely to produce a positive or a negative tag, the negative tagging rate in generic jet is a measure of the mistag probability. This mistag probability is parametrized as a function of jet E_T, jet pseudo-rapidity, and track multiplicity, (see Fig 79). Based on this probability, the number of expected mistagged jets in the $W+$ jets samples is calculated by summing the mistag probabilities for all the jets in the sample.

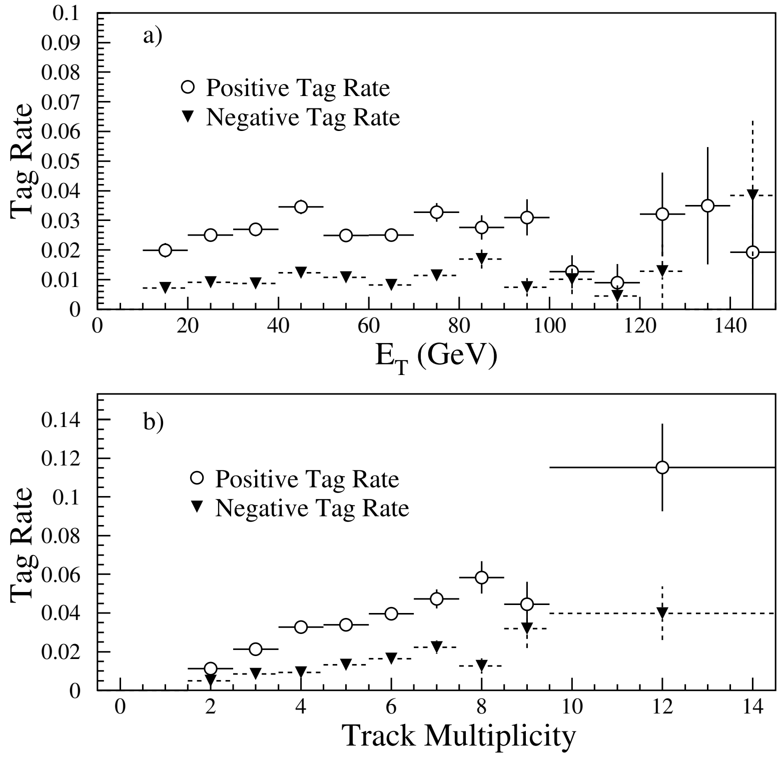

FIG. 79. The tagging rate, defined to be the number of tagged jets divided by the number of jets having two or more tracks with $P_T > 2$ GeV/c reconstructed in the SVX, as a function of (a) the jet E_T, and (b) the number of tracks associated with the jet. Shown are the rates for positive tags (circles) and negative tags (triangles) as measured in a sample of $p\bar{p} \rightarrow$ jets events. The positive tag rate is higher due to the fact that these jets contain a small fraction of heavy quarks (b and c). The positive tag rate is used to calculate the sum of backgrounds due to mistags and $WQ\bar{Q}$ in the Method I background calculation. The negative track rate is used to calculate the mistag background separately in the Method II version of the background calculation. From the CDF collaboration, F. Abe *et al.*, 1994a. Note that these tag rates are not for the final version of the vertex tagging algorithm used by CDF.

The Method II $WQ\bar{Q}$ backgrounds is calculated using theoretical expectations for the rates of $WQ\bar{Q}$. The fraction of W events containing a $Q\bar{Q}$ pair is taken from theory, and multiplied by the number of observed W events to estimate the number of $WQ\bar{Q}$ in the pre-tag samples. The product of this number with the expected $WQ\bar{Q}$ tagging efficiency yields the expected tagged $WQ\bar{Q}$ background. Note that the theoretical input is the fraction of W

Source	$W+$ 1 jet	$W+$ 2 jets	$W+$ 3 jets	$W+\geq$ 4 jets
$WQ\bar{Q}$	13.8 $\pm$ 11.1	7.8 $\pm$ 6.2	2.0 $\pm$ 1.6	0.5 $\pm$ 0.4
Mistags	14.8 $\pm$ 3.0	5.3 $\pm$ 1.1	1.4 $\pm$ 0.3	0.5 $\pm$ 0.1
$W+c$	15.3 $\pm$ 4.6	4.2 $\pm$ 1.3	0.9 $\pm$ 0.4	0.2 $\pm$ 0.1
$Z \rightarrow \tau\tau$, Dibosons	0.8 $\pm$ 0.3	0.8 $\pm$ 0.3	0.2 $\pm$ 0.1	0.04 $\pm$ 0.2
$b\bar{b}$	5.7 $\pm$ 1.4	3.0 $\pm$ 0.8	0.8 $\pm$ 0.2	0.18 $\pm$ 0.04
Total	50 $\pm$ 12	21.1 $\pm$ 6.5	5.2 $\pm$ 1.7	1.45 $\pm$ 0.43
Tagged jets	40	34	17	10

TABLE XII. Summary of Method II backgrounds and tags in the CDF vertex tag analysis (Carithers, 1995). The 27 tags in the $\geq$ 3 jets sample occurr in 21 events. Assuming Standard Model top production, one would expect between approximately 40 (M_{top} = 140 GeV/c^2) and 5 (M_{top} = 200 GeV/c^2) tagged $t\bar{t}$ events in the $\geq$ 3 jets sample.

events that include a $Q\bar{Q}$ pair rather than the much more uncertain absolute rate prediction, see the discussion in Section V.E.4. The $W+c$ background (see Fig. 51) is calculated in a similar manner, i.e. by multiplying the number of $W+$ jets events by the fraction of W events which are expected to contain a single c-quark, and by the tagging efficiency for these events. Other backgrounds, such as $Z \rightarrow \tau\tau$, dibosons, and $b\bar{b}$ are computed mostly from Monte Carlo. The background expectations and event yields are summarized in Table XII, and displayed in Fig. 80

In the $W+\geq$ 3 jets sample, CDF finds 27 tagged jets in 21 events, with a background expectation of 6.7 $\pm$ 2.1 tags. The power of the vertex tag algorithm is such that only 1.9 $\pm$ 0.4 of these tags can be attributed to mistags, see Table XII. The six events with two tagged jets can be compared with four expected for the top + background hypothesis, and $\leq$ 1 for background alone. Furthermore, six of the vertex tagged events also include a lepton tag. This is in much better agreement with expectations for top + background (about four events) than with background alone (about one event). As further evidence of a b-contribution to this sample, the proper time distribution for tagged jets is also found to be consistent with expectations from b-jets, see the inset of Fig. 80. As we will show in Section VIII.E, the size of the excess is consistent with expectations from $t\bar{t}$ for a top mass in the neighborhood of 160 GeV/c^2.

The Method II background calculation in the $W+$ 1 jet sample is in good agreement with the data, providing a very important check of the reliability of the background estimation. We note that the Method I background estimate in the $W+$ 1 jet sample yields 80 $\pm$ 10 tags, in clear disagreement with the observed 40 tags. In the $W+$ 2 jets sample, the Method II background calculation is lower than the number of tags observed in the data. However, approximately 5 tags from $t\bar{t}$ are expected in this sample based on the excess of tags seen in the higher jet multiplicity samples. After accounting for these events, the background calculation in the $W+$ 2 jet sample is then found to be in satisfactory agreement with the data.

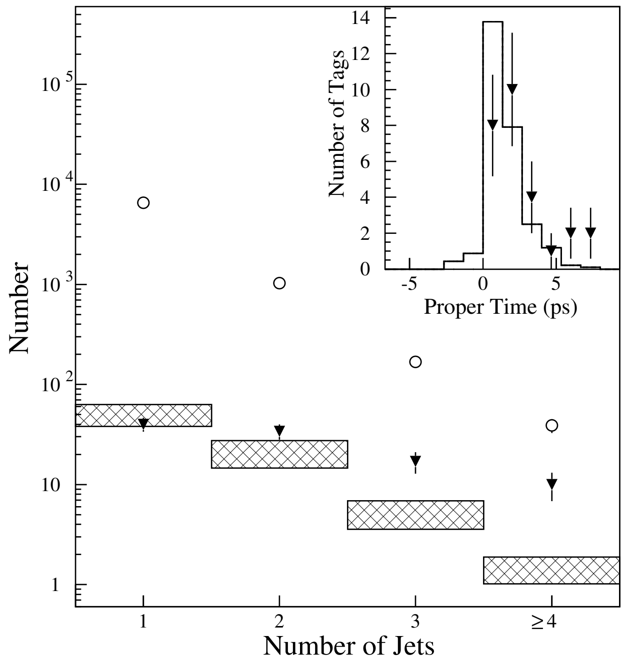

FIG. 80. Number of events before vertex tagging (circles), number of tags observed (triangles), and expected number of background tags (hatched) as a function of jet multiplicity. The inset shows the secondary vertex proper time distribution for the 27 tagged jets in the $W+\geq 3$ jets data (triangles) compared to the expectation for b-quark jets from $t\bar{t}$ decays. From the CDF collaboration, F. Abe *et al.*, 1995a.

4. Summary and cross checks of the tagging background calculation on $Z+$ jets

Samples of $Z+$ jets in principle provide an ideal testing ground for the calculation of tagging backgrounds in the $W+$ jets sample. The properties of jets in W and Z events are very similar, due to the similarities in the W and Z production mechanism. One exception is that whereas in W events $Q\bar{Q}$ pairs can be produced only through gluon splitting, see Fig. 52, in Z events additional mechanisms are also expected to contribute (e.g. $gg \to Zb\bar{b}$, see Fig. 81). A study of expected tagging rates in W or Z + 4 jets, including a model that approximates experimental efficiencies and backgrounds, indicates that the probabilities of tagging a W or a Z event are expected to be the same within 10-15% (Barger *et al.*, 1994).

Unfortunately, the combined cross-section times branching ratio for $p\bar{p} \to Z \to ll$ is

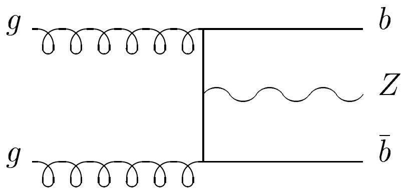

FIG. 81. Feynman diagram for $gg \to Zb\bar{b}$.